Bioorganic Chemistry 89 (2019) 102992

Contents lists available at ScienceDirect

Bioorganic Chemistry

journal homepage: www.elsevier.com/locate/bioorg

Pharmacological investigation of quinoxaline-bisthiazoles as multitarget-directed ligands for the treatment of Alzheimer's disease

Sneha R. Sagar[a,c], Devendra Pratap Singh[b,1], Rajesh D. Das[a], Nirupa B. Panchal[a,c], Vasudevan Sudarsanam[a], Manish Nivsarkar[b], Kamala K. Vasu[a,*]

[a] Department of Medicinal Chemistry, B. V. Patel Pharmaceutical Education and Research Development (PERD) Centre, S. G. Highway, Thaltej, Ahmedabad 380054, Gujarat, India

[b] Department of Pharmacology and Toxicology, B. V. Patel Pharmaceutical Education and Research Development (PERD) Centre, S. G. Highway, Thaltej, Ahmedabad 380054, Gujarat, India

[c] Institute of Pharmacy, NIRMA University, S. G. Highway, Chandlodia, Gota, Ahmedabad 82481, Gujarat, India

ARTICLE INFO

Keywords:
Quinoxalines
Thiazoles
BACE-1
Inflammation
Multitarget-directed ligands

ABSTRACT

Alzheimer's disease (AD) is the most prevalent disease of old age leading to dementia. Complex AD pathogenesis involves multiple factors *viz.* amyloid plaque formation, neurofibrillary tangles and inflammation. Herein we report of a new series of quinoxaline-bisthiazoles as multitarget-directed ligands (MTDLs) targeting BACE-1 and inflammation concurrently. Virtual screening of a library of novel quinoxaline-bisthiazoles was performed by docking studies. The most active molecules from the docking library were taken up for synthesis and characterized by spectral data. Compounds **8a-8n** showed BACE-1 inhibition in micro molar range. One of the compounds, **8n** showed BACE-1 inhibition at IC_{50} of 3 ± 0.07 μM. Rat paw edema inhibition in acute and chronic models of inflammation were obtained at 69 ± 0.45% and 55 ± 0.7%, respectively. Compound **8n** also showed noteworthy results in $AlCl_3$ induced AD model. The treated rats exhibited excellent antiamnesic, antiamyloid, antioxidant, and neuroprotective properties. Behavioural parameters suggested improved cognitive functions which further validates the testimony of present study. Moreover, compound **8n** was found to have inherent gastrointestinal safety. This new string of quinoxaline-bisthiazoles were identified as effective lead for the generation of potent MTDLs and compound **8n** was found to showcase qualities to tackle AD pathogenesis.

1. Introduction

Alzheimer's disease (AD) is chronic, irreversible and the most prevalent neurodegenerative disorder of the brain concomitant to old age and currently accounts over 46.8 million cases of dementia worldwide [1–3]. Primarily characterized by exacerbated cognitive dysfunction and irreversible memory impairment. Clinically, AD can be explicated as mild to severe cognitive decline accompanied by gradual dysfunction both in memory and areas of higher intellectual functions such as linguistic skills, judgments in complicated situations and basic routine works. Major victims of AD are people of the age groups of 65 years and older; however the onset may occur earlier during their 40 s or 50 s which remains un-noticed. In 2015, there were as many as 46.8 million cases of dementia globally and projections are likely that this figure may double every 20 years, rising to 74.7 million by 2030 and 131.5 million by 2050 if an efficient systematic treatment methodology is not developed [4].

Although no substantial evidences to compel the exact pathophysiology of AD are yet identified, certain epidemiological and preliminary researches largely attribute the underlying mechanism to two major hallmarks *viz.* (i) β-amyloid (Aβ) plaques and (ii) neurofibrillary tangles (NFTs) [5]. Additionally, other factors affecting the pathophysiology of this malady in some way or the other are inflammation, excitotoxicity, neurotransmitter imbalance, oxidative stress, elevated cholesterol level, dysregulation of biometal ions (especially Cu^{+2}, Zn^{+2} and Fe^{+2}), etc. [6,7]. The treatment of AD has endured a challenge for

Abbreviations: AD, Alzheimer's disease; MTDLs, multitarget-directed ligands; BACE-1, β-site APP cleaving enzyme-1; APP, amyloid precursor protein; Aβ, amyloid β; NFTs, neurofibrillary tangles; COXs, cyclooxygenases; NC, normal control; DC, disease control; PC, positive control; r.t, room temperature; BBB, blood brain barrier; HERG, Human Ether-à-go-go-Related Gene; LPO, lipid peroxidation; SOD, superoxide dismutase

* Corresponding author.
E-mail addresses: kamkva@gmail.com, kamalav@perdcentre.com (K.K. Vasu).
[1] Present address: Manager R&D, (FDD-NDDS), Sun Pharmaceutical Industries Limited, Tandalija, Vadodara, Gujarat, India.

https://doi.org/10.1016/j.bioorg.2019.102992
Received 10 November 2018; Received in revised form 7 April 2019; Accepted 17 May 2019
Available online 22 May 2019

the pharmaceutical community as yet. The pathology of AD is intricately cumbersome owing to its association with abnormality and dysfunction of multisystem. Thus, the prevention and real cure have been elusive till date and its molecular etiology still remains enigmatic. Current pharmacotherapy being palliative in nature prompts timely symptomatic relief and ameliorates patient's condition but do not produce profound disease modifying effects.

Accordingly, the search for viable disease modifying agents could be addressed by shifting the drug discovery paradigm from single to multitarget-directed ligands which are more requisite in addressing the labyrinthine nature of the disease. The MTDL strategy has emerged as a powerful drug design exemplar after the multitarget approach started on the discovery of multiple activities of natural products such as curcumin, resveratrol and some flavonoids [8]. Ever since the benefits of MTDLs therapy over single target drug design were noticed, a lot of MTDLs were studied to combat the disease modifying complications associated with AD [9–19]. In this connection, we arrived at a cognizance that there is an unmet need to develop antiamyloid therapy as well which can hit distinct molecular targets of the neurodegenerative cascade [20–22]. In this study, we have designed MTDLs acting upon amyloid pathway enzyme *viz.* β-site APP cleaving enzyme (BACE)-1 and inflammation. Our study aims at combining two scaffolds into one single molecule to generate potential lead for complex AD intervention.

A retrospection of the concept of amyloid hypothesis revealed that the amyloid precursor protein (APP) gets cleaved by two different pathways: "non-amyloidogenic" and "amyloidogenic" [23]. Non amyloidogenic pathways were not detected to be involved in Aβ generation whereas amyloidogenic pathway products were found to be primarily responsible for the formation of β-amyloid plaques. The APP first gets cleaved by β-secretase enzyme and subsequently by γ-secretase provoking the release of β-amyloid into the extracellular cerebral site. Consequently, the cleaved products of APP form amyloid-β (Aβ) peptides: $A\beta_{40}$ and $A\beta_{42}$. Of these, $A\beta_{42}$ is identified as immensely neurotoxic and participates in plaque formation in the pathogenesis of AD [5,24]. Besides the amyloid plaque formation, an activation of inflammatory processes also affects the progression of AD. An inference made from the available literature is that pro-inflammatory substances like reactive oxygen species (ROS), interleukin (IL) 1 & 6, tumor necrosis factor (TNF) and cyclooxygenases (COXs) play a major role in degeneration and death of the neuronal cells [25]. In short, we can conclude that BACE-1 is fundamentally responsible for the generation of neurotoxic β-amyloid (Aβ) peptide which is broadly considered to have a crucial early role in etiology of AD. As a result, BACE-1 has originated as a key drug target to taper the extension of toxic Aβ in the AD brain, and the development of BACE-1 and inflammation inhibitors as therapeutic agents is being eagerly executed. The morbid pathophysiology of BACE-1 and neuronal inflammation in AD is pictured in Fig. 1.

1.1. Design of molecules

The therapeutic profiles of various MTDLs explored so far, seem to confer with the ability of quinoxalines arising as a useful ring scaffold in AD therapy. For example, 1-(2,3-di(furan-2-yl)quinoxalin-6-yl)-3-(3-hydroxypropyl)urea (**1**) showed inhibition of tau fibrillization with IC_{50} of 2.4 μM [27]. Hexyl 2-cyano-2-(3-(4-methylpiperazin-1-yl)quinoxalin-2-yl)acetate (**2**) was also evaluated as inhibitor of tau, α-synuclein and amyloid $\beta_{1\text{-}42}$. IC_{50} of the compound (**2**) against tau protein and amyloid $\beta_{1\text{-}42}$ was obtained at 2.8 μM and 0.76 μM, respectively [28]. *N*-(3-aminoquinoxalin-2-yl)-4-(piperidin-1-ylmethyl)benzamide (**3**) showed 47% inhibition of BACE-1 at 20 μg/mL concentration [29]. These scaffolds warrant the therapeutic ability of quinoxalines against AD which is further demonstrated in Fig. 2. Additionally, our lab has a profound interest in exploring various heterocycles like thiazoles, thiophenes, and quinazolinones in varied therapeutic regions [30–32]. As a result, potent anti-inflammatory properties of thiazoles have been proven in *in vivo* rat model. Ethyl (5-((hydroxyimino)(4-(methylsulfonyl)phenyl)methyl)-4-methylthiazol-2-yl)carbamate (**4**) showed substantial anti-inflammatory activity with 69% inhibition of rat paw edema in acute inflammation [30]. *N*,*N*′-(5,5′-oxalylbis(4-methylthiazole-5,2-diyl))dibenzamide (**5**) showed 73% inhibition of edema in acute inflammation model [30]. The collaborative assembly of two ring scaffolds into a single molecule to act as BACE-1 and inflammation inhibitor is portrayed in Fig. 2.

2. Results & discussion

The present study encapsulates development of such chemical entities featuring abilities to hit multiple targets associated with AD. The string of prototype MTDLs designed in this study showed remarkable inhibition of BACE-1 enzymatic pathway and also exposed potential anti-inflammatory tendencies. To delineate this fact, *in silico* docking studies, *in vitro*, *in vivo* and GI safety studies have been carried out comprehensively and the interpretation of the results have been discussed in following sections.

2.1. Molecular docking

The rationale of the present work was initiated by molecular docking studies [33]. A library of molecules was scrutinized by *in silico* docking studies employing BACE-1, BACE-2, Cathepsin D, COX-1 and COX-2 enzymes to predict the binding affinity. To achieve selectivity towards BACE-1 over BACE-2 and Cathepsin D, binding interaction with the catalytic pocket of BACE-1 was mandatory. The catalytic pocket of BACE-1 has an aspartic dyad at the centre which forms hydrogen bonding network in the active site. The molecular docking study bespoke that some of the molecules displayed binding interactions with the aspartic dyad of BACE-1. Lower binding affinity towards BACE-2 and Cathepsin-D was beneficial to get the selective BACE-1 inhibition as non-selective inhibition may lead to the cell death therefore only molecules selectively inhibiting BACE-1 over BACE-2 and Cathepsin-D were further assessed. Additionally, docking studies on inflammatory pathway enzymes COX-1 and COX-2 were carried out. Higher binding affinity and docking score for COX-1 and COX-2 was advantageous. From the library of designed compounds, 14 molecules **8a-n** were selected for further studies. The results of *in silico* screening of designed MTDLs for BACE-1 inhibitory and anti-inflammatory pathways are depicted in Table 1. From the virtual library, compounds **8a-n** showed higher binding affinity with BACE-1, COX-1 and COX-2 enzymes. Compounds with lesser docking score values are incorporated in Supplementary Material.

The binding interactions of compound **8n** against BACE-1 and COX-2 enzymes are pictured in Fig. 3. Fig. 3A illustrates an overlay of docked compound **8n** and BACE-1 inhibitor AZD3839 (reference molecule) with BACE-1 enzyme's catalytic active site. AZD3839 showed H-bonding interactions with catalytic aspartic dyad Asp32 and Asp228. In addition, it also interacted with Phe108 and Trp76. π-π stacking interaction was observed with amino acid residue Tyr71. Similarly, compound **8n** also showed binding interactions with catalytic Asp32, Asp228, Trp76 and Tyr71. Docking score value obtained for AZD3839 and compound **8n** was found to be −8.8 and −7.8, respectively. Fig. 3B illustrates an overlay of docked compound **8n** and a COX-2 inhibitor celecoxib with COX-2 enzyme's catalytic region. The H-bonding interactions with amino acids Leu338, Ser339 and Phe504 and π-cation interaction with Arg106 were observed for celecoxib whereas in case of compound **8n** interactions were observed with Phe504, Leu338 and Arg106.

2.2. Physicochemical properties prediction

Drug likeliness prediction of drugs targeting BBB is an important criteria to look into. Qikprop module of Schrödinger was used for the

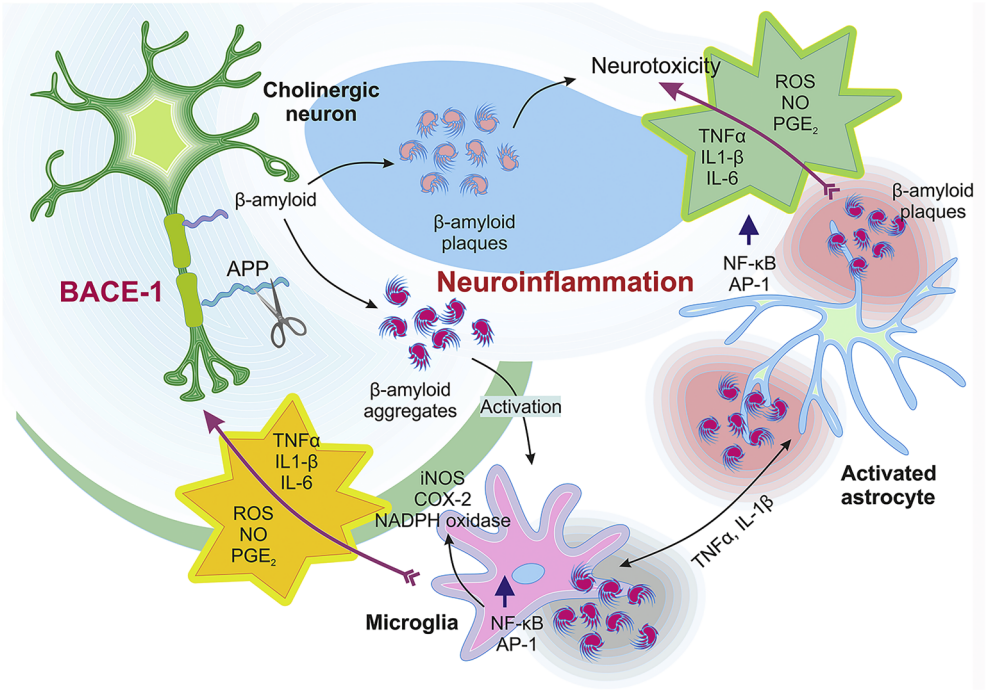

Fig. 1. Pathogenesis of Alzheimer's disease [26].

prediction of physicochemical properties (Table 2) [34]. Molecules obeyed the Lipinski's rule of five and Jorgensen's rule of three. They showed drug likeliness properties with higher BBB permeation and lower toxicity according to HERG inhibition which is evident from Table 2. Physicochemical parameters like, QPlogPo/w, QPlogBB, % HOA, QPPCaco and QPlogHERG are enlisted in Table 2.

2.3. Chemistry

The active compounds identified through docking studies were synthesized as per scheme mentioned in Fig. 4. The substituted 2,3-bis (bromomethyl)quinoxalines **2a-c** were obtained by reaction of substituted benzene-1,2-diamines **1a-c** with 1,4-dibromobutane-2,3-dione

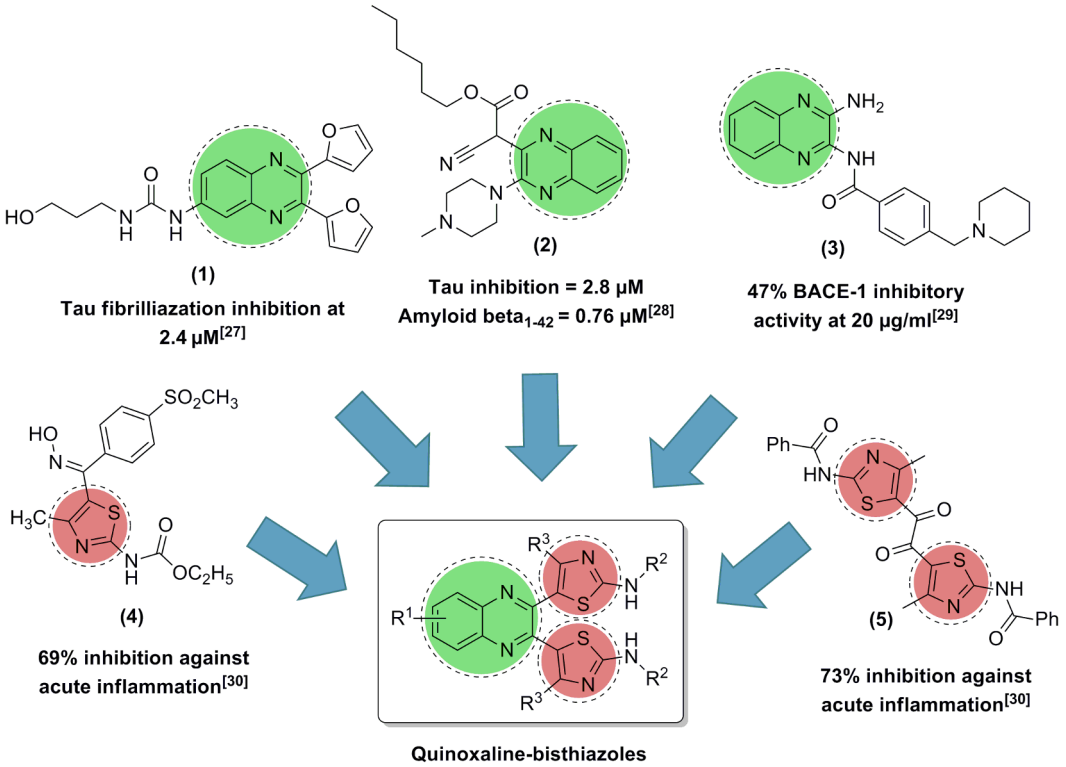

Fig. 2. Design strategy for a novel series of MTDLs in AD.

Table 1
Results of docking studies (See Table 3 for specific substitutions).

Code	Docking Score				
	BACE-1	BACE-2	Cathepsin D	COX-1	COX-2
8a	−7.4	−3.8	−2.9	−7.8	−7.0
8b	−7.6	−4.4	−4.2	−7.6	−7.3
8c	−6.8	−4.8	−3.4	−6.9	−6.5
8d	−6.7	−4.1	−4.2	−7.0	−6.8
8e	−5.7	−4.3	−4.4	−6.5	−6.1
8f	−6.0	−4.5	−4.6	−6.4	−6.4
8g	−7.2	−3.5	−3.9	−8.0	−7.1
8h	−5.9	−4.4	−4.0	−6.2	−6.6
8i	−6.3	−4.7	−4.1	−6.1	−6.0
8j	−6.6	−4.0	−3.4	−6.7	−6.7
8k	−5.8	−3.6	−4.5	−5.9	−6.0
8l	−7.6	−3.9	−3.2	−7.2	−7.4
8m	−6.1	−4.9	−4.8	−6.0	−6.7
8n	−7.8	−4.0	−4.2	−7.5	−8.3
AZD3839	**−8.8**	−4.3	−4.4	−5.6	−5.5
Diclofenac	−3.6	−3.2	−3.5	**−8.7**	**−8.4**
Celecoxib	−4.9	−4.7	−4.5	−11.8	**−12.2**
Hydroxyethylenamine inhibitor	−5.2	**−11.8**	−4.6	−4.2	−5.0

in ethanol at 0 °C for 2 h. To afford intermediates *N*′-carbamothioylformimidamides **4a-d**, carboxamidines **3a-c** were reacted with various isothiocyanates in tetrahydrofuran at room temperature for about 3 to 4 h [35,36]. Synthesis of substituted *N*′-carbamothioyl-*N*,*N*-dimethylformimidamides **6a-e** was carried out via reaction of substituted thiourea **5a-e** with 1,1-dimethoxy-*N*,*N*-dimethylmethanamine in methanol for 2 h at ambient temperature. The treatment of substituted 2,3-bis(bromomethyl)quinoxalines **2a-c** with substituted *N*′-carbamothioylformimidamides **4b-d** afforded tritylated intermediates **7a-f.** Upon deprotection with trifluoro acetic acid final compounds **8a-f** were obtained. Also, intermediates **2a-c** were reacted with **4a** and **6a-e** to produce final compounds **8g-n**.

On the basis of ^{1}H NMR spectra of intermediates **2a** and **4a**, the formation of final compound **8g** can be explained. Intermediate **2a**, 2,3-bis(bromomethyl)quinoxaline has molecular formula of $C_{10}H_8Br_2N_2$. Its ^{1}H NMR spectra shows a singlet at 4.338 δ (a) which corresponds to four protons of two –CH_2 groups. Further, a triplet of two protons is obtained at 7.331 δ (b) and a doublet of two protons is obtained at chemical shift value of 7.821 δ (c) (see Supplementary Material). An another intermediate, *N*,*N*-diethyl-*N*′-(phenylcarbamothioyl)benzimidamide **4a** has molecular formula of $C_{18}H_{21}N_3S$. The ^{1}H NMR spectra of this compound shows a triplet of two –CH_3 groups (6H) at chemical shift of 1.089 δ (a′). A quartet peak is obtained at 3.187 δ corresponds to four protons of two –CH_2 groups (b′). In the aromatic region, peaks corresponding to two phenylic protons are obtained as multiplet at 7.142–7.472 δ (c′ to g′). A singlet for proton corresponding to –NH group is obtained at 10.290 δ (h′) (see Supplementary Material).

The final compound 5,5′-(quinoxaline-2,3-diyl)bis(*N*,4-diphenylthiazol-2-amine) **8g** has molecular formula of $C_{38}H_{26}N_6S_2$. Compound **8g** is formed by reaction of intermediate **2a** (1 eq) with intermediate **4a** (2 eq). In compound **8g**, two –CH_2 group's peak of intermediate **2a** (a) is disappeared as it is now cyclized to form thiazole scaffold. Also, peaks of –CH_2-CH_3 group disappeared in final compound's spectra (a' and b') which were seen in case of intermediate **4a** (–$N(CH_3)_2$ group acts as readily leaving group upon cyclization). Importantly, there are four phenyl groups in compound **8g** and the corresponding aromatic protons are obtained in the range of 6.97–7.83 δ (20H, a″ to g″). Additionally, peaks of protons present in the quinoxaline ring scaffold remain unchanged as in case of **2a** (4H, f″ and g″). In **8g**, there is a singlet peak corresponding to two –NH group protons (h″) (see Supplementary Material).

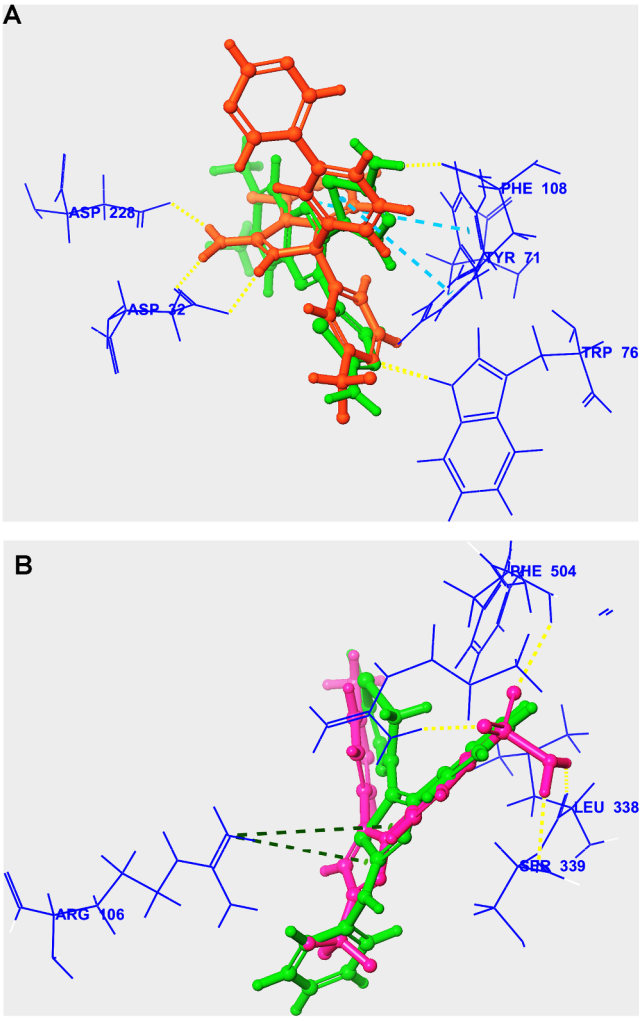

Fig. 3. Docking study results. (A) Overlay of compound **8n** (green sticks) with AZD3839 (orange sticks): AZD3839 showed H-bonding interactions (Yellow dotted line) with Asp32, Asp228, Trp76 and Phe108 and π-π stacking interaction (cyan dotted line) with Tyr71. Compound **8n** interacted with Asp32, Asp228, Trp76 and Tyr71. (B) Overlay of compound **8n** (green sticks) with Celecoxib (pink sticks): Celecoxib showed H-bonding interactions (Yellow dotted line) with Leu338, Ser339 and Phe504 and π-cation interaction (green dotted line) with Arg106. Compound **8n** also interacted with Phe504, Leu338 and Arg106.

2.4. Biological activity

2.4.1. In vitro BACE-1 enzyme inhibition assay

The therapeutic profile of MTDLs as BACE-1 inhibitor was practically assessed by FRET based *in vitro* enzymatic assay. All the synthesized compounds (**8a-8n**) were evaluated for their BACE-1 enzyme inhibitory activity and the results were compared with the clinical candidate's (AZD3839) reported value. IC_{50} values in terms of μM ± SEM (n = 3) are enlisted in Table 3. Results suggested that all compounds inhibited BACE-1 enzyme in micro molar range. Compounds **8b**, **8l** and **8n** were found have maximal potency with IC_{50} equivalent to 4, 8 and 3 μM, respectively. This consequence of high potency can be attributed to their high binding affinity with BACE-1 enzyme which was previously evaluated from docking study. Compound **8k** and **8m** showed minimal potency with IC_{50} values above 100 μM. Compounds **8a**, **8c**, **8d**, **8e**, **8f**, **8g**, **8h**, **8i**, and **8j** showed moderate inhibition of BACE-1 enzyme. In order to inhibit BACE-1 enzyme, one of the structural features required is –NH_2 functionality as it forms tight H-bond with catalytic aspartic acids Asp32 and Asp228 of

Table 2
Physicochemical properties prediction.

Code	QPlogPo/w[a]	QPlogBB[b]	%HOA[c]	QPPCaco[d]	QPlogHERG[e]
8a	2.03	−1.22	80	189	−5.24
8b	4.39	−1.29	95	234	−8.16
8c	3.34	−1.24	91	294	−5.94
8d	3.21	−1.16	87	292	−5.07
8e	3.27	−1.02	90	294	−5.94
8f	2.50	−1.09	82	190	−5.17
8g	6.00	−0.44	100	2756	−10.25
8h	1.36	−1.29	74	146	−5.43
8i	5.48	−0.52	100	1414	−7.37
8j	5.78	−0.25	92	1622	−6.82
8k	6.21	−0.24	94	1457	−6.99
8l	1.82	−1.16	76	145	−5.37
8m	5.89	−0.50	92	1461	−6.90
8n	1.89	−1.39	77	144	−5.32
AZD3839	4.35	−0.629	100	500	−6.42
Diclofenac	4.50	−0.155	100	398	−2.95
Celecoxib	3.34	−0.780	92	358	−5.78

[a] QPlogPo/w: Predicted octanol/water partition coefficient (−2.0 to 6.5).
[b] QPlogBB: Predicted brain/blood partition coefficient (−3.0 to 1.2).
[c] %HOA: Predicted human oral absorption (> 80% is high, < 25% is poor).
[d] QPPCaco: Predicted Caco-2 cell permeability (< 25 poor, > 500 great).
[e] QPlogHERG: Predicted IC_{50} value for blockage of HERG K + channels (below −5).

BACE-1 enzyme. The substitution at R^2 position gives less active compounds (see Table 3). Quinoxaline ring scaffold is responsible for π-π stacking interaction with Tyr71. Nitrogen of thiazole ring is also significant for H-bonding interactions with Trp76. In addition, substitution at R^3 position with -$N(CH_3)_2$ group did not give potent BACE-1 inhibition as in case of compounds **8c**, **8d** and **8e**. BACE-1 inhibition was hardly affected by the substitution at R^1 position.

2.4.2. *In vivo analysis*

2.4.2.1. Acute anti-inflammatory activity: Carrageenan induced rat paw edema study. In addition, the anti-inflammatory potential of these MTDLs was tested by studying rat model of acute and chronic inflammation. All 14 molecules were examined via carrageenan induced acute inflammation model. A subcutaneous injection of carrageenan induces inflammation by metabolism of arachidonic acid. This causes plasma and leukocyte extravasations, increased tissue water and plasma protein exudation along with neutrophil extravasations. The above inflammatory event was diminished by our string of MTDLs at 50 mg·kg^{-1} dose. Compounds **8c**, **8i**, **8l** and **8n** showed anti-inflammatory activity with % edema inhibition of 60%, 55%, 57% and 69%, respectively. On the contrary, standard drug diclofenac given at a dose of 7.5 mg kg^{-1} showed edema inhibition of 72% (see Table 3).

2.4.2.2. Chronic anti-inflammatory activity: Formalin induced rat paw edema study. Further, the most active molecules obtained from *in*

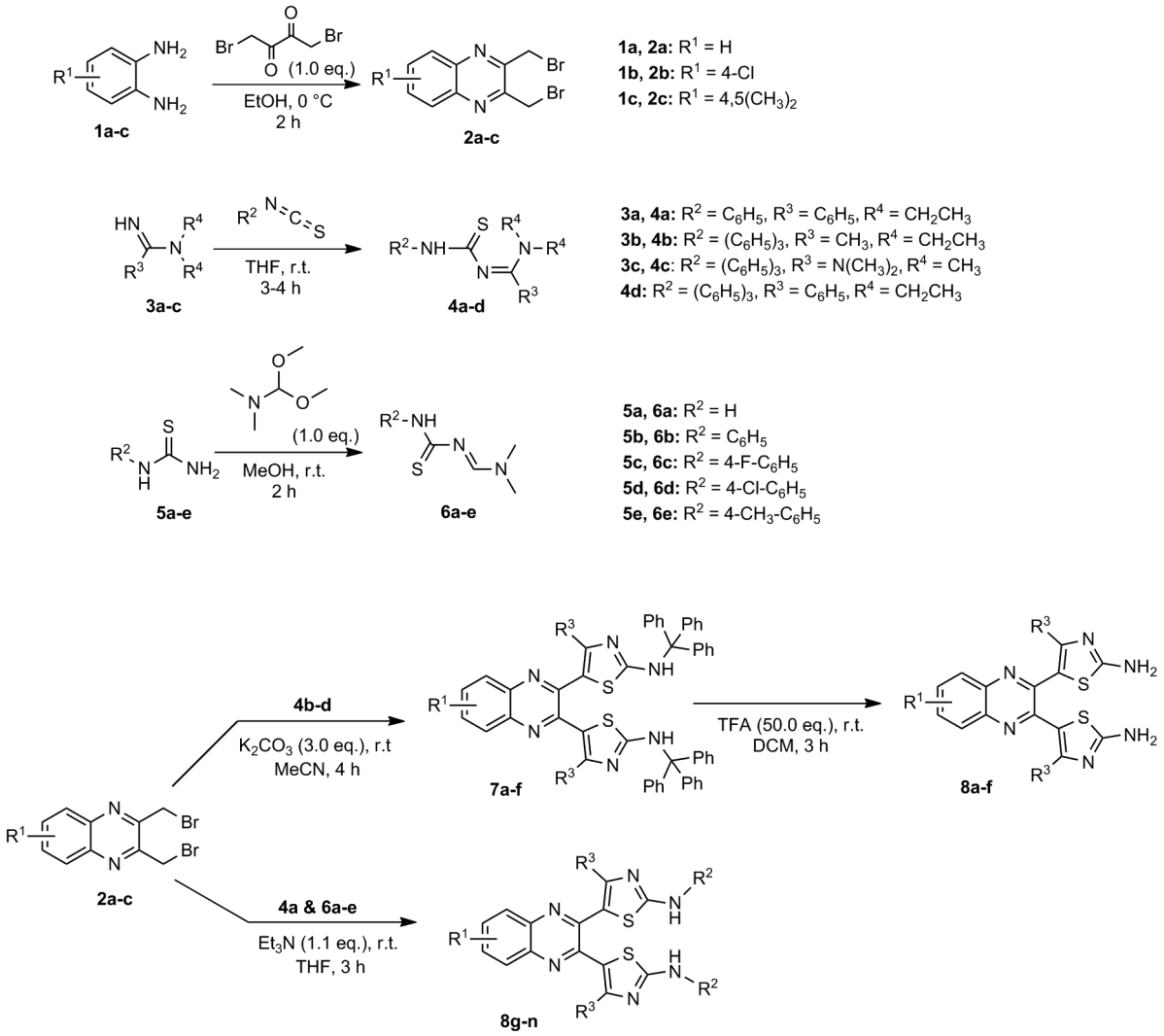

Fig. 4. Synthetic scheme of quinoxaline-bisthiazoles.

Table 3
List of synthesized compounds with BACE-1 inhibition assay results and % inhibition of edema in acute inflammation model.

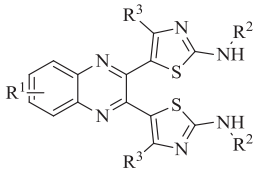

Code	R^1	R^2	R^3	IC_{50} (μM) ± SEM[a]	% inhibition of paw edema [mean ± SEM][b]
8a	H	H	CH_3	16 ± 0.09	33 ± 1.45
8b	H	H	C_6H_5	4 ± 0.60	38 ± 0.70
8c	3,4-$(CH_3)_2$	H	$N(CH_3)_2$	32 ± 0.40	60 ± 0.50
8d	H	H	$N(CH_3)_2$	92 ± 0.30	39 ± 0.70
8e	4-Cl	H	$N(CH_3)_2$	90 ± 0.08	35 ± 1.35
8f	4-Cl	H	CH_3	31 ± 0.67	32 ± 1.05
8g	H	C_6H_5	C_6H_5	27 ± 0.02	48 ± 0.70
8h	H	H	H	90 ± 0.80	48 ± 1.55
8i	H	C_6H_5	H	42 ± 0.80	54 ± 0.80
8j	H	4-F-C_6H_5	H	30 ± 0.90	19 ± 1.40
8k	H	4-Cl-C_6H_5	H	112 ± 0.50	28 ± 1.50
8l	Cl	H	H	8 ± 0.50	57 ± 0.55
8m	H	CH_3	H	110 ± 0.50	17 ± 1.10
8n	3,4-$(CH_3)_2$	H	H	3 ± 0.07	69 ± 0.45
Diclofenac				NT	72 ± 0.65

NT not tested.
[a] IC_{50} is the concentration (μM) required to inhibit 50% of BACE-1 enzyme. All values are expressed as mean of three replicates ± SEM.
[b] Data presented as the % inhibition of paw edema relative to the DC group. Statistical analysis was performed by One-way ANOVA followed by Tukey's multiple comparison test. Mean ± SEM (n = 6 animals/group) *p < 0.05.

vitro BACE-1 assay and *in vivo* acute inflammatory studies i.e. compounds **8c**, **8g**, **8l**, and **8n** were taken forward to chronic model of inflammation. Formalin induces early neurogenic response followed by tissue mediated responses by releasing histamine, 5-HT, kinin and prostaglandins. A formalin induced chronic rat paw edema model was developed and molecules were tested consecutively for 5 days. The results indicated the % edema inhibition of 28%, 49%, 31% and 55%, respectively at a dose of 50 mg kg^{-1}. In this instance, the standard drug celecoxib (40 mg kg^{-1}) given to rats showed 68% edema inhibition when tested under same conditions and parameters. The results are shown in Table 4.

One of the structural features required for the anti-inflammatory activity is indeed the presence of thiazole ring moiety as ring nitrogen forms H-bond with both COX-1 and COX-2 enzymes. Moreover, anti-inflammatory activity is favored by $–NH_2$ functional group as seen in compounds **8c**, **8l** and **8n**. Substitution at R^1 position was not majorly affected by different groups. At R^3 position, $–CH_3$ and -C_6H_5 groups did not favor the anti-inflammatory activity so, no substitution is required there.

The most optimal hybrid molecule **8n** resulting from BACE-1 inhibition assay, acute and chronic inflammation model was further taken up to analyze its anti-Alzheimer's activity by employing $AlCl_3$ induced AD model. Compound **8n** was screened by behavioural parameters, antioxidant property and histopathological studies.

2.4.2.3. Behavioural parameters

2.4.2.3.1. Y-maze test. Simultaneous alteration performance (SAP) was determined using Y-maze apparatus and % alteration was calculated [37]. During acquisition session, rats in all the groups showed preference for novel environment and higher % alteration as depicted in Fig. 5A. There was no significant difference of % alteration during this period. In contrast, on 7th, 14th, 21st and 28th day DC group animals showed significant decrease in the % alteration parameter compared to the NC group ($^{*}p < 0.05$). Treatment with compound **8n** reduced the amnesic effect aroused from $AlCl_3$ injections and significantly improved % alteration ($^{\#}p < 0.05$).

2.4.2.3.2. Conditioned avoidance response test. Using pole climbing apparatus, conditioned avoidance response (CAR) was evaluated in all test groups. During the acquisition time, rats learned to escape from the foot shock and showed low CAR (*sec*) values. None of the groups showed any significant differences of CAR during acquisition session, whereas on day 7th, 14th, 21st and 28th day of the test session, CAR substantially increased in DC group rats when compared to NC rats ($^{*}p < 0.05$). Treatment with compound **8n** improved the learning memory of rats and showed significant decrease in the CAR, contrary to which is observed in DC group rats ($^{\#}p < 0.05$) as shown in Fig. 5B.

2.4.2.3.3. Elevated plus maze test. Spatial working memory of rats was investigated using EPM test [38]. Time (s) consumed by each rat to travel from an open arm to a closed arm (transfer latency) was recorded. During training period, none of the rats showed any significant difference in their transfer latency after having memorized the path. Further, $AlCl_3$ treatment in DC group rats significantly increased the transfer latencies ($^{*}p < 0.05$) on 7th, 14th, 21st and 28th day and the rats took more time to reach a closed arm from an open arm than they usually did in training sessions. Improvement in spatial working memory was noted in compound **8n** treated rats and they showed significant decrease in transfer latency ($^{\#}p < 0.05$) compared to DC group rats, as depicted in Fig. 5C.

2.4.2.4. Haematological parameters estimation. After 28 days of $AlCl_3$ dosing, on the 29th day haematological parameters were observed [39]. Haemoglobin and haematocrit levels were estimated using automated haematology analyser. From the results of the mentioned study, it was observed that there was a significant reduction in haemoglobin and haematocrit level in PC rats ($^{*}p < 0.05$) as given in Fig. 5D & E. The cause of decrease in the haemoglobin and haematocrit can be attributed to the gastric ulcers present in rat's stomach in meloxicam treated group. Treatment with compound **8n** did not show decrease in haemoglobin and haematocrit level. These results were further validated by gastrointestinal lesion index study.

Table 4
% edema inhibition against formalin induced chronic inflammation.

Compound	%inhibition of edema in chronic inflammation model [mean ± SEM][a]				
	Day 1	Day 2	Day 3	Day 4	Day 5
8c	31 ± 1.8	33 ± 1.3	36 ± 1.4	29 ± 1.5	28 ± 1.6
8g	37 ± 1.2	43 ± 1.4	47 ± 1.8	42 ± 1.8	49 ± 2.0
8l	42 ± 2.0	43 ± 1.7	39 ± 1.4	33 ± 1.7	31 ± 2.4
8n	49 ± 1.9	63 ± 2.2	61 ± 1.3	56 ± 2.0	55 ± 1.4
Celecoxib	67 ± 1.8	74 ± 1.1	70 ± 2.4	70 ± 1.9	68 ± 1.0

[a] Data expressed as the % inhibition of paw edema relative to the DC group. Statistical analysis was performed by One-way ANOVA followed by Tukey's multiple comparison test. Mean ± SEM (n = 6 animals/group) *p < 0.05.

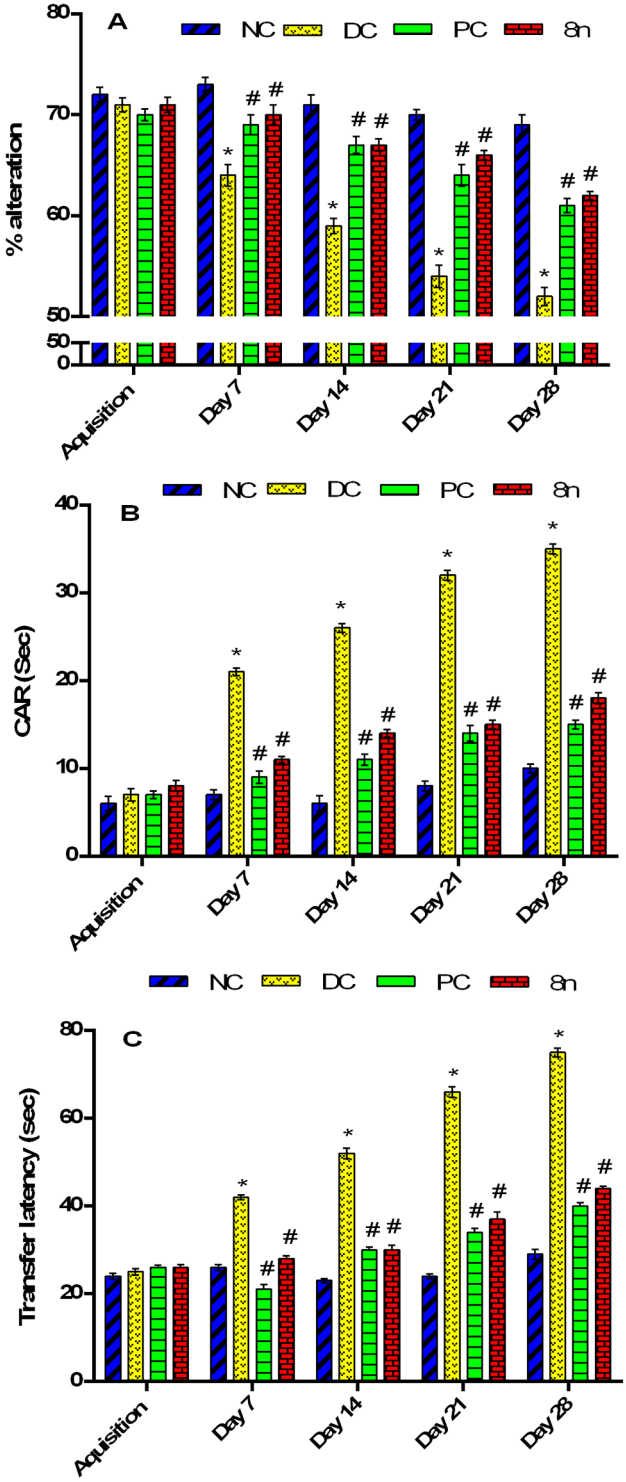

Fig. 5A–C. Behavioral parameters estimation. (**A**) Results of Y maze test expressed as % alteration (**B**) results of conditioned avoidance response (CAR) using pole climbing apparatus (**C**) results of transfer latency using elevated plus maze test. Data expressed as mean ± SEM. Asterisk denotes statistical significance (*p < 0.05) when compared to NC group and ($^{\#}$p < 0.05) when compared to DC group, using two-way ANOVA followed by Tukey's multiple comparison test.

2.4.2.5. Estimation of serum biochemical parameters. Serum biochemical parameters were estimated by albumin and total protein level determination. No significant difference was observed in albumin level in any of the groups (Fig. 5F). Nevertheless, significant reduction in the total protein content (*p < 0.05) were observed in

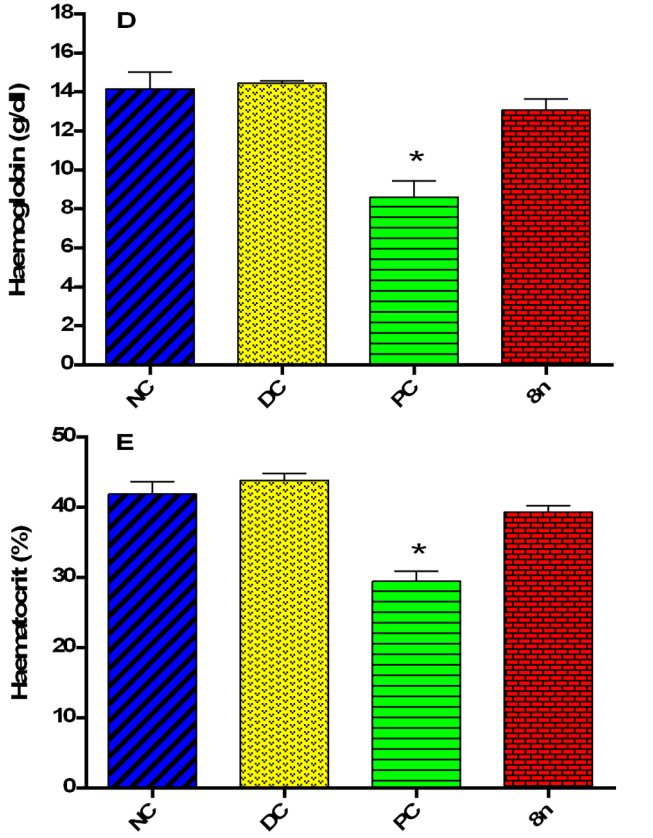

Fig. 5D and E. Estimation of haematological parameters. (**D**) Estimation of haemoglobin (HGB) level (**E**) Results of haematocrit (HCT) level. Data expressed as mean ± SEM (*p < 0.05) by using one-way ANOVA followed by Tukey's multiple comparison test.

PC rats as evident from Fig. 5G. DC group and compound **8n** treated rats did not show any reduction in total protein level.

2.4.2.6. Antioxidant activity. The *in vivo* antioxidant activity was checked by lipid peroxidase assay (LPO) and superoxide dismutase assay (SOD). Rat brain homogenates were subjected to MDA level determination using UV/Visible spectrophotometer (Shimadzu UV-1800). MDA is an oxidative marker which indicates oxidative damage of tissues. Aluminium causes oxidative damage in conjunction with copper and iron and significantly increases the level of LPO in rat brain tissues. The mechanism underlying the increase in LPO production is the stabilization of iron by aluminium in its reduced state (Fe^{2+}). $AlCl_3$ induction increased the oxidative stress and stimulated MDA level increment in DC animals. In contrast, treatment with **8n** significantly reduced MDA level compared to the DC rats ($^{\#}$p < 0.05) as shown in Fig. 5H. In addition to this, $AlCl_3$ also causes oxidative stress induced tissue damage by significant decrease in SOD activity. SOD value was significantly increased in compound **8n** treated rats in comparison to DC group rats ($^{\#}$p < 0.05) as depicted in Fig. 5I. Importantly, the overall results of these studies indicates that compound **8n** showed promising free radical scavenging effects in the rat brain.

2.4.2.7. Histopathological studies of rat brain. Histopathological evaluation of brain samples was carried out using Haematoxylin-Eosin (HE) stain and Congo red stain. HE stained brain sections were observed under 100× magnified microscope and hippocampal region was closely examined (Fig. 6A). NC rats were seen to have intact healthy neurons in their hippocampus whereas, the DC group showed signs of degeneration (indicated by an arrow). The PC group rats did not showed any degeneration but slight thin hippocampal region was

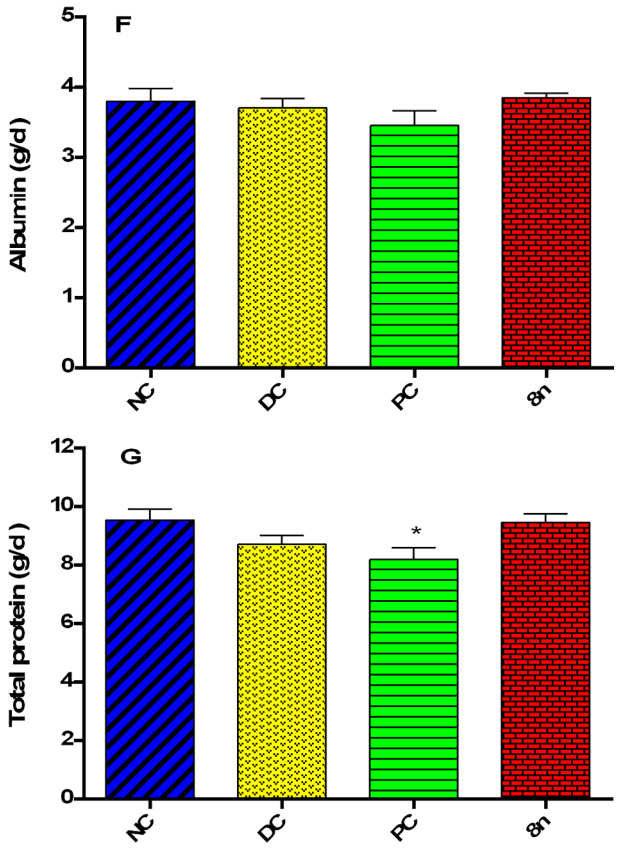

Fig. 5F and G. Estimation of serum biochemical parameters. (**F**) Estimation of serum albumin level (**G**) Estimation of total protein level. Data expressed as mean ± SEM (*p < 0.05) by using one-way ANOVA followed by Tukey's multiple comparison test.

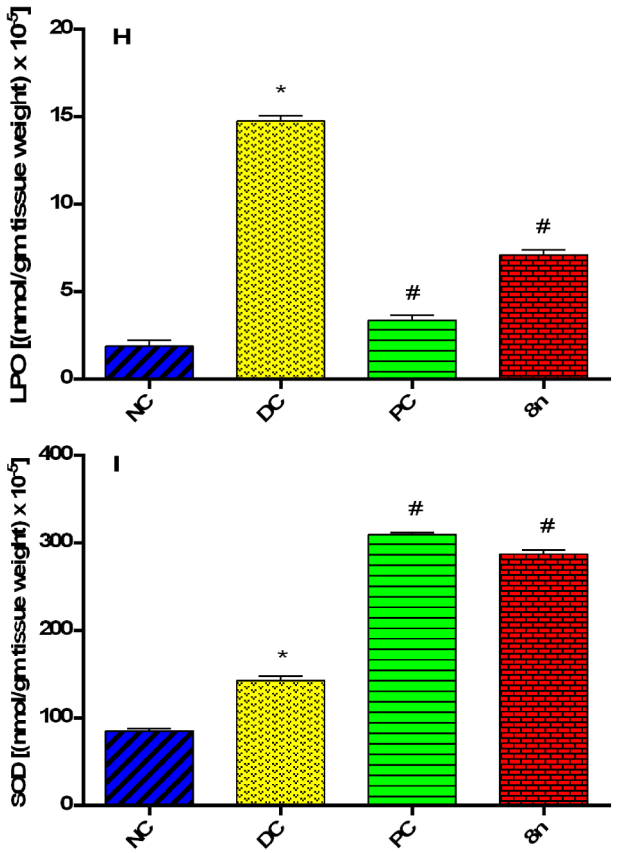

Fig. 5H and I. Anti-oxidative effect of compound **8n.** (**H**) Results of lipid peroxidation (LPO) assay expressed as MDA level (**I**) Estimation of super oxide dismutase (SOD) activity in rat brain homogenate. Data presented as mean ± SEM (n = 6 animals/group) *p < 0.05 compared to NC group and $^{\#}$p < 0.05 when compared to DC group using one-way ANOVA followed by Tukey's multiple comparison test.

observed. Interestingly, compound **8n** treated rats had an intact and healthy hippocampus in their brain indicating that **8n** protected neurons from degeneration. Thus, results of this study signify the neuro-protective benefits of compound **8n.** Further, antiamyloid potential of compound **8n** was estimated by using Congo red stain (Fig. 6B). In the NC group brain cortex, no amyloid plaques were observed but the DC group had amyloid plaques in their cortex region. No plaques were observed in PC group and **8n** treated rats as depicted in Fig. 6B.

2.4.2.8. Gastrointestinal (GI) safety study. Nonsteroidal anti-inflammatory drugs (NSAIDs) have an inherent risk of causing gastro-enteropathic damage to the GI track. On the contrary, test compound **8n** interestingly didn't show any signs of GI damage. To check this aspect, macroscopic and microscopic evaluation of gastrointestinal tract were carried out on 29th day of $AlCl_3$ model. The internal portions of stomach and intestines were examined and lesion indices were calculated for all rats. Control group animals did not show any gastric damage in their stomach or intestines, whereas, PC group rats had lesions in their stomach (lesion index = 12.19 ± 0.8 mm) and intestines (lesion index = 29.15 ± 1.6 mm). Compound **8n** treated rats did not show any lesions in their intestine, however a small damage was observed in the stomach region (lesion index = 3.07 ± 0.35 mm) as shown in Fig. 6C. Although compound **8n** showed promising anti-inflammatory activity, gastric damage was minimal as compared to the standard drug meloxicam. The gastric damage in stomach and intestinal sections were further checked up by microscopic evaluation using HE stain. NC and DC group rats did not show any erosions in their stomachs (see Fig. 6D) and intestines (see Fig. 6E). PC group rats were noticed to have severe gastric injuries with focal erosions in stomach and epithelium erosion and stratification in intestines. Importantly, compound **8n** treated rats showed minor focal erosion in their stomach but no damage was observed in intestines.

3. Conclusion

The amyloidogenic cascade theory of Alzheimer's disease suggest that secretases, the enzyme acting upon β-APP facilitates the emanation of Aβ peptides and apparently emerges as one of the key contributors in AD aetiology. The amyloid plaques and damaged neurons induce the release of TNF-α, IL-1β, COXs and many other inflammatory cytokines leading to neuronal cell degeneration and cell death. Therefore, BACE-1 promotion and neuronal cell inflammation are critical processes related to the development of AD. Hence, it can be logically concluded that BACE-1 inhibitory and anti-inflammatory leads can function as a therapeutic paragon in AD intervention. The ongoing research circulates around development of disease-modifying therapies targeting BACE-1 and inflammation for the treatment of AD. Quinoxaline and thiazole scaffolds were conjugated owing to their BACE-1 inhibitory and anti-inflammatory responses to develop novel MTDLs. *In silico* docking studies of library of quinoxaline-bisthiazoles suggested their multitargeted profile. Compounds were found to interact with catalytic pocket of BACE-1, COX-1 and COX-2 whereas, least binding score was obtained for BACE-2 and Cathepsin D enzymes. Compounds were taken further for *in vitro* BACE-1 inhibition assay and *in vivo* acute and chronic inflammation studies. Taken together, the outcomes from *in silico*, *in vitro* and *in vivo* studies, compound **8n** emerged as the most potent MTDL. In $AlCl_3$ induced AD model, compound **8n** showed promising antiamnesic,

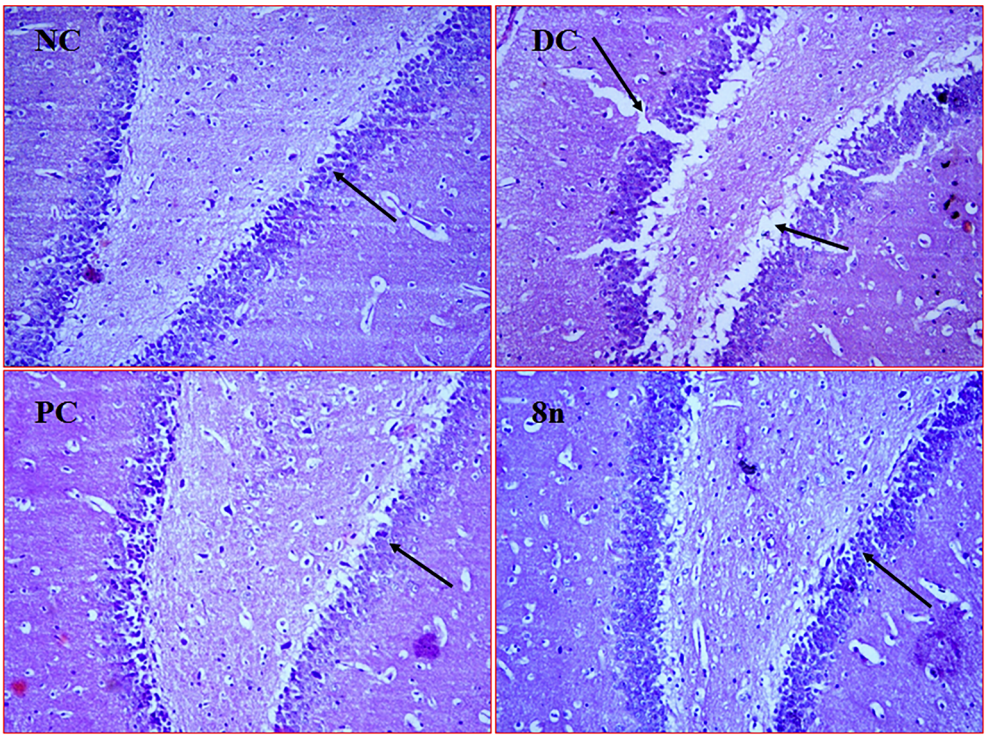

Fig. 6A. Typical microscopic HE stained sections (100× magnification) of brain hippocampus. **NC** group rats with healthy and intact hippocampus, **DC** group rats had ruptured hippocampus and degenerated neuronal cells, **PC** rats showed intact hippocampal region and Compound **8n** treated rats with normal and healthy neuronal cells in hippocampal region.

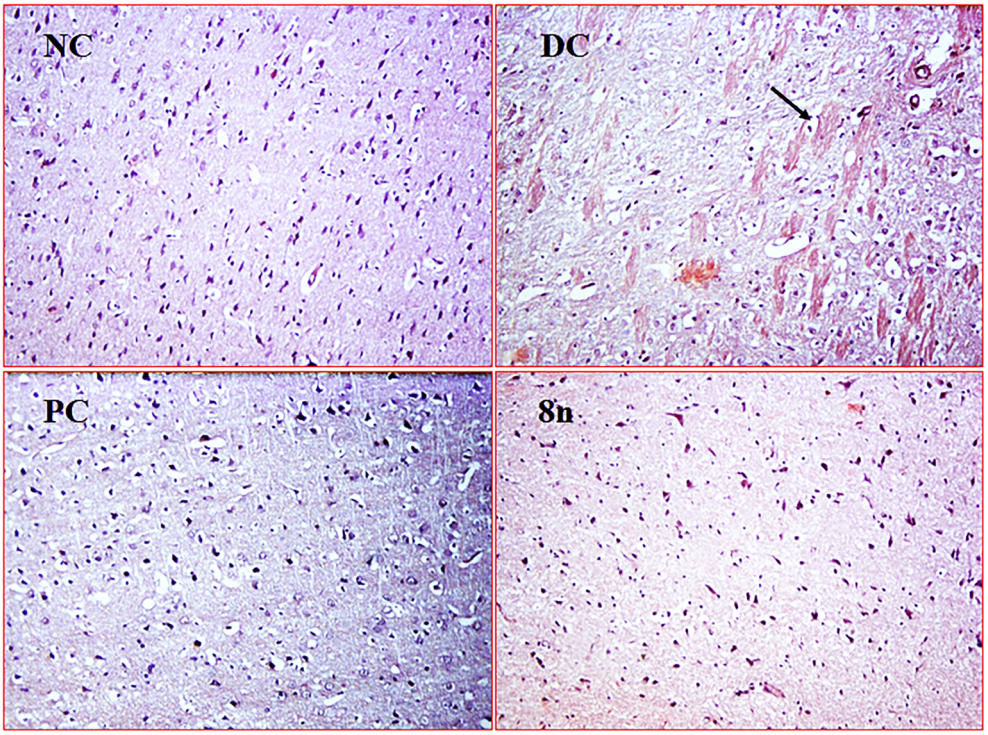

Fig. 6B. Congo red stained sections (100× magnification) of brain cortex. **NC** group rat's brain cortex without any amyloid plaques, Amyloid plaques were present in the cortex of **DC** group rats (stained red) indicated by an arrow, **PC** group rats without plaques and Compound **8n** treated brain cortex did not show amyloid plaques.

antioxidant, antiamyloid and neuroprotective attributes. In addition, despite having potent anti-inflammatory benefits, this molecule hardly shows any GI toxicity unlike other NSAIDS. The functional consequences of targeting BACE-1 inhibitory and anti-inflammatory pathways turned out to be of pragmatic relevance to attempt restoration of cognitive dysfunction with disease modifying properties related to AD pathology. In future, compound **8n** may emerge as promising MTDL in clinical studies.

4. Materials and methods

4.1. Molecular docking studies

Prior to the *in silico* evaluation, three-dimensional X-ray crystal structures of proteins required for analysis were downloaded from the protein-data-bank. To evaluate the binding modes of compounds, docking studies were carried out using Maestro 11.1.012 program of

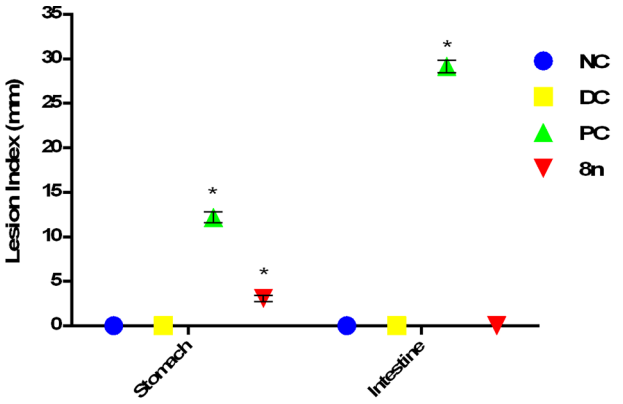

Fig. 6C. Macroscopic evaluation of gastric damage by lesion index. Data given as mean ± SEM (*$p < 0.05$) by using two-way ANOVA followed by Tukey's multiple comparison test.

Schrödinger, LLC, New York, NY, 2017, USA. Structures of various quinoxaline-bisthiazoles with different R^1, R^2 and R^3 substitutions were fed into the software (see Table 1 and Supplementary material). A meticulous virtual screening of these fabricated molecules was performed to rationalize their feasible inhibitory tendencies against BACE-1 and inflammatory pathway enzymes. Out of these, the molecules with best docking score values amongst BACE-1, COX-1 and COX-2 were selected for further assessment (See Table 1). Amongst these, the molecules displaying lesser docking score for BACE-2 and Cathepsin D were chosen so as to procure selectivity of BACE-1 over BACE-2 and Cathepsin D.

Ligand preparation: All molecules were drawn and cleaned up in the Maestro 2D sketcher software. The Ligprep module was employed for energy minimization by OPLS3 force field and possible states were obtained using Epik (pH 7.0).

Protein preparation: To prepare **BACE-1 protein,** a crystal structure containing coherent structure of BACE-1 bound ligand AZD3839 (clinical candidate) was retrieved from protein-data-bank (PDB ID: 4B05) [40]. The protein structure was constructed using protein preparation wizard of Schrödinger 11.1.012 software. Bond orders were assigned and hydrogens were added to the structures. Subsequently, zero-order bonds to metals and to disulfide bonds were added. Missing side chains were affixed using prime and water molecules within 5 Å of het groups were removed. All ions were deleted and protein structures were optimized using OPLS3 force field and minimized for receptor grid generation which was obtained at the centroid of the ligand (AZD3839) of BACE-1 receptor. Likewise, protein structure for **BACE-2** was constructed using the crystal structure of human BACE-2 receptor (PDBID: 2EWY) bound to hydroxyl-ethylenamine transition-state inhibitor [45]. The crystal structure of Cathepsin D (PDB ID: 1LYW) was used for docking process [46]. Binding sites were generated by using SiteMap module [47] in Schrödinger. Amongst the top ranked potential binding sites identified by using SiteScore, the topmost binding site was selected for receptor grid generation. Grid was generated at the binding site pocket of the Cathepsin D enzyme and then used for the docking process.

Cyclooxygenases protein preparation: Crystal structure of COX-1 in complexation with Celecoxib (PDB ID: 3KK6) and COX-2 with co-crystallized Celecoxib ligand (PDB ID: 3LN1) were used for the docking process [48,49]. All the steps for the protein preparation were followed as described in BACE-1 protein preparation protocol using chain A of the enzyme.

Docking study: Ligand docking was brought out using Glide module of Schrödinger suite and extra precision (XP) mode was applied for the docking of all the molecules with proteins. Docking score and interactions of ligands with protein were considered for activity prognosis of the molecules. Re-docking of co-crystallized ligand with the proteins was brought to operation for precise validation of docking process [33].

4.2. Physicochemical properties prediction

Physicochemical properties of all compounds were virtually perceived by using QikProp application of Schrödinger software. Drug

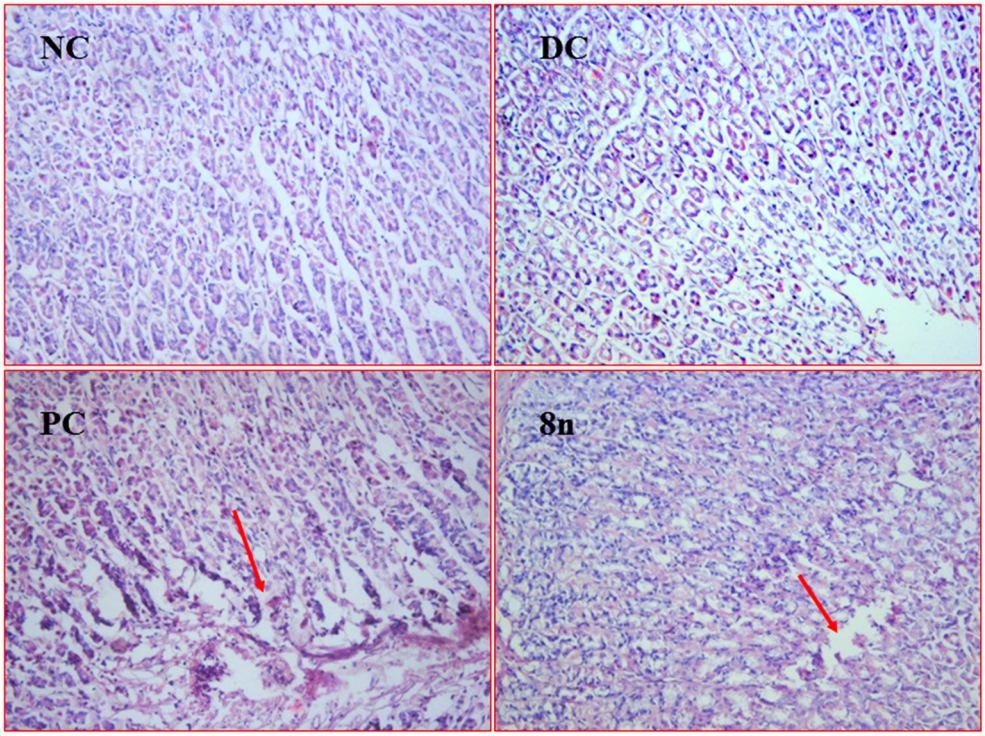

Fig. 6D. Typical microscopic HE stained sections (under 100× magnification) of rat stomach. No stomach erosions present in **NC** rats, **DC** group rats without any erosions, **PC** rats stomach had large focal erosions (indicated by an arrow), compound **8n** treated rats had little erosions (indicated by an arrow).

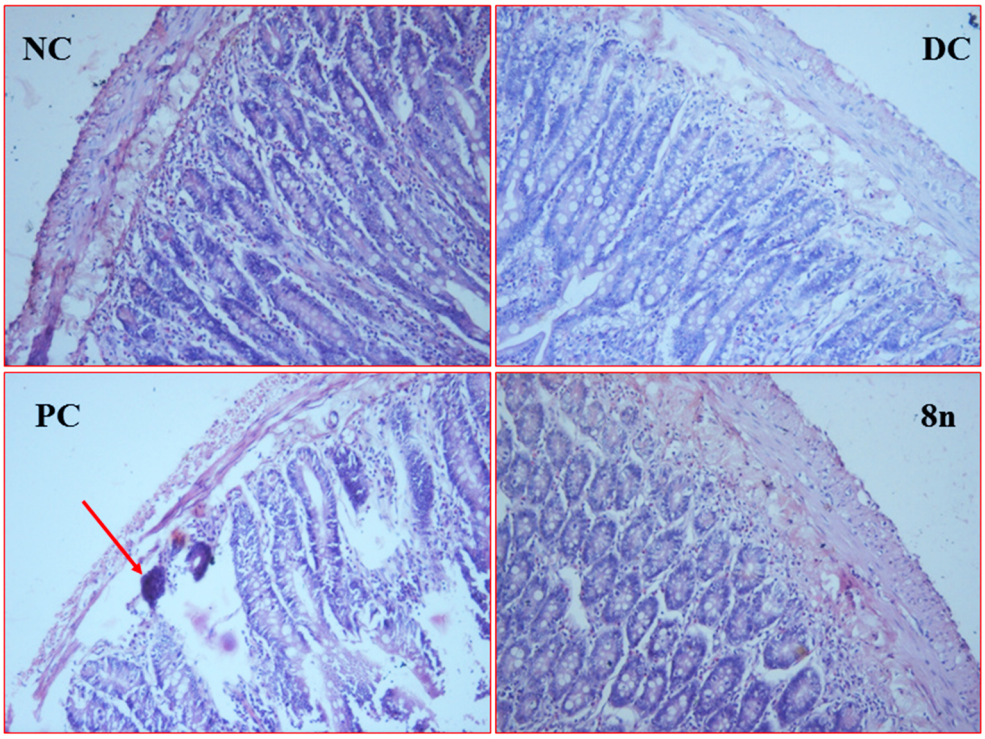

Fig. 6E. Typical microscopic HE stained sections (under 100× magnification) of rat intestine. **NC** group rats did not show gastric damage, **DC** group rats without any focal erosions, **PC** group rats showed focal erosions of the superficial epithelium and epithelial stratification indicated by an arrow, No erosions or epithelium stratification was observed in compound **8n** treated animals.

likeliness properties such as octanol/water partition coefficient (QPlogPo/w), brain/blood partition coefficient (QPlogBB), % human oral absorption (HOA), Caco-2 cell permeability (QPPCaco) and HERG inhibition (QPlogHERG) were taken into evaluation to foretell brain permeability and toxicity of the molecules [34].

4.3. Chemistry

4.3.1. General methods

Unless stated otherwise, all starting material, reagents and solvents were purchased from commercial suppliers Spectrochem, Sigma-Aldrich, Fisher Scientific, HiMedia and used without any further purification. To check the progress of reaction, thin layer chromatography (TLC) was employed using ready-made silica gel plates (pre-coated, Merck) and visualized under ultraviolet lamp. Melting points (°C) were obtained using scientific melting point apparatus (Veego; Model VMP-DS) and are uncorrected. Column chromatography was carried out using 100–200 mesh silica gel. To check the purity of compounds HPLC was carried out using SHIMADZU-LC-2010. Shimadzu's IR Affinity 1 was used to record FTIR spectra. Mass spectra were obtained by using Perkin Elmer Mass Spectrometer and values are quoted in *m/z*. HRMS analysis was done by Q-TOF micromass (ESI-MS). ^{1}H NMR and ^{13}C NMR spectra were recorded using Bruker Avance II 400 MHz NMR spectrophotometer. Chemical shift values are represented in parts per million (ppm) in δ-scale. Coupling constant (*J*) values were observed in Hertz (Hz). Fine splitting of the signals are described as s (singlet), d (doublet), t (triplet), q (quartet), m (multiplet) and dd (doublet of doublets).

4.3.2. Synthesis

*4.3.2.1. Synthesis and characterization of substituted 2,3-bis (bromomethyl)quinoxalines **(2a-c)***

*4.3.2.1.1. 2,3-Bis(bromomethyl)quinoxaline **(2a)**.* To the solution of benzene-1,2-diamine (1.0 eq) **1a** in ethanol, 1,4-dibromobutane-2,3-dione (1.0 eq) was added slowly. Reaction temperature was maintained at 0 °C. Reaction mixture was allowed to stir for 2 h. After completion of reaction, ethanol was evaporated *in vacuo* to get dried compound **2a**. Pale green solid; Yield: 75%; Melting point: 151–153 °C; LC-ESI-MS (*m/z*): 313.9 $[M]^+$, 315.9 $[M+2]^+$, 317.9 $[M+4]^+$.

*4.3.2.1.2. 2,3-Bis(bromomethyl)-6-chloroquinoxaline **(2b)**.* Intermediate **2b** was prepared by the procedure described in **2a** using 4-chlorobenzene-1,2-diamine **1b**. Yield: 71%; Light pink solid; Melting point: 174–176 °C; LC-ESI-MS (*m/z*): 347.9 $[M]^+$, 349.9 $[M+2]^+$, 351.9 $[M+4]^+$, 353.9 $[M+6]^+$.

*4.3.2.1.3. 2,3-Bis(bromomethyl)-6,7-dimethylquinoxaline **(2c)**.* Intermediate **2c** was prepared by the procedure described in **2a** using 4,5-dimethylbenzene-1,2-diamine **1c**. Yield: 74%; Light pink solid; Melting point: 181–183 °C; LC-ESI-MS (*m/z*): 341.9 $[M]^+$, 343.9 $[M+2]^+$, 345.9 $[M+4]^+$.

*4.3.2.2. Synthesis and characterization of substituted N'-carbamothioylformimidamide **(4a-d)***

*4.3.2.2.1. N,N-diethyl-N'-(phenylcarbamothioyl)benzimidamide **(4a)**.* To the solution of *N,N*-diethylbenzimidamide **3a** (1.0 eq) in THF, addition of isothiocyanatobenzene (1.0 eq) was done. Reaction was allowed to proceed at room temperature for 3–4 h. After completion of reaction, THF was evaporated *in vacuo* to get pale yellow solid of **4a**. **4a** was used without further purification. Yield: 81%; Pale yellow solid; Melting point: 195–197 °C; LC-ESI-MS (*m/z*): 312.1 $[M+H]^+$.

*4.3.2.2.2. N,N-diethyl-N'-(tritylcarbamothioyl)acetimidamide **(4b)**.* Intermediate **4b** was prepared by the procedure described in **4a** using (isothiocyanatomethanetriyl)tribenzene and *N,N*-diethylacetimidamide **3b**. Yield: 70%; Colorless solid; Melting point: 188–190 °C; LC-ESI-MS (*m/z*): 416.2 $[M+H]^+$.

*4.3.2.2.3. 1-(Bis(dimethylamino)methylene)-3-tritylthiourea **(4c)**.* Intermediate **4c** was prepared by the procedure described in **4a** using (isothiocyanatomethanetriyl)tribenzene and 1,1,3,3-tetramethylguanidine **3c**. Yield: 86%; Pale yellow solid; Melting point: 182–184 °C; LC-ESI-MS (*m/z*): 417.2 $[M+H]^+$.

*4.3.2.2.4. N,N-diethyl-N'-(tritylcarbamothioyl)benzimidamide **(4d)**.* Intermediate **4d** was prepared by the procedure described in **4a** using (isothiocyanatomethanetriyl)tribenzene and *N,N*-diethylbenzimidamide **3a.** Yield: 82%; Melting point: 195–197 °C; LC-ESI-MS (*m/z*): 478.2 $[M+H]^+$.

*4.3.2.3. Synthesis and characterization of substituted N'-carbamothioyl-N,N-dimethylformimidamide (**6a-e**)*

*4.3.2.3.1. N'-carbamothioyl-N,N-dimethylformimidamide (**6a**)*. Thiourea **5a** (1.0 eq) in methanol was reacted with 1,1-dimethoxy-*N,N*-dimethylmethanamine (2.0 eq) at room temperature for 3 h to get *N*'-carbamothioyl-*N,N*-dimethylformimidamide **6a.** After completion of reaction, methanol was evaporated *in vacuo* to get compound **6a**. **6a** was used without further purification. Yield: 85%; Pale yellow solid; Melting point: 202–204 °C; LC-ESI-MS (*m/z*): 132.1 $[M+H]^+$.

*4.3.2.3.2. N,N-dimethyl-N'-(phenylcarbamothioyl)formimidamide (**6b**)*. Intermediate **6b** was prepared by the procedure described in **6a** using 1-phenylthiourea **5b.** Yield: 79%; Melting point: 195–197 °C; LC-ESI-MS (*m/z*): 208.2 $[M+H]^+$.

*4.3.2.3.3. N'-((4-fluorophenyl)carbamothioyl)-N,N-dimethylformimidamide (**6c**)*. Intermediate **6c** was prepared by the procedure described in **6a** using 1-(4-fluorophenyl)thiourea **5c.** Yield: 71%; Melting point: 208–210 °C; LC-ESI-MS (*m/z*): 226.2 $[M+H]^+$.

*4.3.2.3.4. N'-((4-chlorophenyl)carbamothioyl)-N,N-dimethylformimidamide (**6d**)*. Intermediate **6d** was prepared by the procedure described in **6a** using 1-(4-chlorophenyl)thiourea **5d.** Yield: 73%; Melting point: 211–213 °C; LC-ESI-MS (*m/z*): 241.5 $[M]^+$, 243.5 $[M+2]^+$.

*4.3.2.3.5. N,N-dimethyl-N'-(p-tolylcarbamothioyl)formimidamide (**6e**)*. Intermediate **6e** was prepared by the procedure described in **6a** using 1-(p-tolyl)thiourea **5e.** Yield: 78%; Melting point: 204–206 °C; LC-ESI-MS (*m/z*): 221.1 $[M+H]^+$.

*4.3.2.4. Synthesis and characterization of final compounds: Substituted 5,5′-(quinoxaline-2,3-diyl)bis(thiazol-2-amine) (**8a-f**)*

*4.3.2.4.1. 5,5′-(quinoxaline-2,3-diyl)bis(4-methylthiazol-2-amine) (**8a**)*. To a solution of 2,3-bis(bromomethyl)quinoxaline (1.0 eq) **2a** in acetonitrile, K_2CO_3 (3.0 eq) was added. Reaction mixture was allowed to stir and addition of *N,N*-diethyl-*N*'-(tritylcarbamothioyl) acetimidamide **4b** (2.0 eq) was done. Reaction was allowed to proceed at room temperature for 4 h. After completion of reaction, reaction mixture was poured into ice cold water to get the precipitates of tritylated **7a**. Deprotection of tritylated **7a** was done using trifluoro acetic acid (50.0 eq) in DCM for 3 h. After completion of reaction, reaction mixture was poured into ice cold water. Solution was neutralized with sodium bicarbonate to get deprotected final compound **8a**. **8a** was purified by column chromatography (Chloroform: Methanol = 9.5:0.5). Yellow solid; Yield: 76%; Purity: 99.8%; Melting point: 150–152 °C; Molecular formula: $C_{16}H_{14}N_6S_2$; LC-ESI-MS (*m/z*): 355.1 $[M+H]^+$; HRMS (TOF) *m/z* calcd for $C_{16}H_{14}N_6S_2$ $[M+H]^+$ 355.0721, found: 355.0824; IR (KBr, cm^{-1}): 3469.994, 3329.14, 3062.96, 1681.93, 1490.97, 1157.24; ^1H NMR (400 MHz, DMSO-d_6) *δ*: 2.452 (s, 6H), 7.601 (s, D_2O exchangeable, 4H), 7.684 (t, *J* = 3.2 Hz, 2H), 7.865 (d, *J* = 6.4 Hz, 2H); ^{13}C NMR (400 MHz, DMSO-d_6) *δ*: 15.07 (2C), 127.30 (2C), 127.43 (2C), 127.67 (2C), 141.72 (2C), 144.79 (2C), 147.70 (2C), 171.28 (2C).

*4.3.2.4.2. 5,5′-(quinoxaline-2,3-diyl)bis(4-phenylthiazol-2-amine) (**8b**)*. Final compound **8b** was synthesized as per the procedure described in **8a** using starting materials 2,3-bis(bromomethyl) quinoxaline **2a** and *N,N*-diethyl-*N*'-(tritylcarbamothioyl) benzimidamide **4d**. **8b** was purified by column chromatography (Ethyl acetate: Hexane = 7:3). Yellow solid; Yield: 58%; Purity: 99.1%; Melting point: 190–192 °C; Molecular formula: $C_{26}H_{18}N_6S_2$; LC-ESI-MS (*m/z*): 479.1 $[M+H]^+$; IR (KBr, cm^{-1}): 3475.73, 3359.18, 3061.03, 3022.45, 1489.05; ^1H NMR (400 MHz, DMSO-d_6) *δ*: 7.151 (s, D_2O exchangeable, 4H), 7.477 (t, *J* = 7.6 Hz, 2H), 7.560 (t, *J* = 6.8 Hz, 4H), 7.633–7.698 (m, 8H); ^{13}C NMR (400 MHz, DMSO-d_6) *δ*: 117.76 (2C), 120.51 (2C), 123.11 (2C), 125.92 (2C), 128.56 (2C), 129.12 (2C), 129.50 (2C), 131.39 (2C), 137.61 (2C), 137.95 (2C), 141.87 (2C), 155.11 (2C), 170.42 (2C).

*4.3.2.4.3. 5,5′-(6,7-dimethylquinoxaline-2,3-diyl)bis(N^4,N^4-dimethylthiazole-2,4-diamine) (**8c**)*. Final compound **8c** was synthesized as per the procedure described in **8a** using starting materials 2,3-bis (bromomethyl)-6,7-dimethylquinoxaline **2c** and 1-(bis(dimethylamino) methylene)-3-tritylthiourea **4c**. **8c** was purified by column chromatography (Chloroform: Methanol = 9.5:0.5). Yellow solid; Yield: 74%; Purity: 99.5%; Melting point: 190–192 °C; Molecular formula: $C_{20}H_{24}N_8S_2$; LC-ESI-MS (*m/z*): 441.1 $[M+H]^+$; IR (KBr, cm^{-1}): 3474.91, 3256.16, 2925.17, 1585.55, 760.95; ^1H NMR (400 MHz, DMSO-d_6) *δ*: 2.367 (s, 6H), 3.365 (s, 12H), 7.254 (s, D_2O exchangeable, 4H), 7.539 (s, 2H); ^{13}C NMR (400 MHz, DMSO-d_6) *δ*: 19.64 (2C), 41.30 (4C), 127.49 (2C), 137.19 (2C), 140.42 (2C), 147.74 (2C), 157.92 (2C), 168.43 (2C), 179.38 (2C).

*4.3.2.4.4. 5,5′-(quinoxaline-2,3-diyl)bis(N^4,N^4-dimethylthiazole-2,4-diamine) (**8d**)*. Final compound **8d** was synthesized as per the procedure described in **8a** using starting materials 2,3-bis (bromomethyl)quinoxaline **2a** and 1-(bis(dimethylamino)methylene)-3-tritylthiourea **4c**. **8d** was purified by column chromatography (Chloroform: Methanol = 9.5:0.5). Yellow solid; Yield: 67%; Purity: 99.6%; Melting point: 210–212 °C; Molecular formula: $C_{18}H_{20}N_8S_2$; LC-ESI-MS (*m/z*): 413.2 $[M+H]^+$; IR (KBr, cm^{-1}): 3477.66, 3251.46, 3062.96, 1597.06, 1332.81, 759.95; ^1H NMR (400 MHz, DMSO-d_6) *δ*: 3.365 (s, 12H), 6.966 (s, D_2O exchangeable, 4H), 7.221 (t, *J* = 6.8 Hz, 2H), 7.308 (d, *J* = 6.8 Hz, 2H); ^{13}C NMR (400 MHz, DMSO-d_6) *δ*: 36.16 (4C), 125.55 (2C), 128.47 (2C), 129.05 (2C), 139.10 (2C), 142.44 (2C), 144.93 (2C), 170.24 (2C).

*4.3.2.4.5. 5,5′-(6-chloroquinoxaline-2,3-diyl)bis(N^4,N^4-dimethylthiazole-2,4-diamine) (**8e**)*. Final compound **8e** was synthesized as per the procedure described in **8a** using starting materials 2,3-bis (bromomethyl)-6-chloroquinoxaline **2b** and 1-(bis(dimethylamino) methylene)-3-tritylthiourea **4c**. **8e** was purified by column chromatography (Chloroform: Methanol = 9.5:0.5). Yellow solid; Yield: 72%; Purity: 99.1%; Melting point: > 250 °C; Molecular formula: $C_{18}H_{19}ClN_8S_2$; LC-ESI-MS (*m/z*): 446.5 $[M]^+$, 448.5 $[M+2]^+$; IR (KBr, cm^{-1}): 3455.62, 3294.56, 2927.10, 1562.41, 767.70; ^1H NMR (400 MHz, DMSO-d_6) *δ*: 3.451 (s, 12H), 7.234 (s, D_2O exchangeable, 4H), 7.402 (d, *J* = 9.0 Hz, 1H), 7.621 (d, *J* = 9.0 Hz, 1H), 7.789 (s, 1H); ^{13}C NMR (400 MHz, DMSO-d_6) *δ*: 36.41 (4C), 117.81 (2C), 127.26, 128.13 (2C), 128.72 (2C), 129.25 (2C), 130.34, 139.12, 140.50, 141.34, 169.72.

*4.3.2.4.6. 5,5′-(6-chloroquinoxaline-2,3-diyl)bis(4-methylthiazol-2-amine) (**8f**)*. Final compound **8f** was synthesized as per the procedure described in **8a** using starting materials 2,3-bis(bromomethyl)-6-chloroquinoxaline **2b** and *N,N*-diethyl-*N*'-(tritylcarbamothioyl) acetimidamide **4b**. **8f** was purified by column chromatography (Chloroform: Methanol = 9.5:0.5). Yellow solid; Yield: 76%; Purity: 99.7%; Melting point: 223–225 °C; Molecular formula: $C_{16}H_{13}ClN_6S_2$; LC-ESI-MS (*m/z*): 388.5 $[M]^+$, 390.5 $[M+2]^+$; IR (KBr, cm^{-1}): 3468.61, 3305.99, 3062.96, 1598.99, 700.16; ^1H NMR (400 MHz, DMSO-d_6) *δ*: 2.457 (s, 6H), 7.240 (s, D_2O exchangeable, 4H), 7.402 (d, *J* = 9.0 Hz, 1H), 7.620 (d, *J* = 9.0 Hz, 1H), 7.789 (s, 1H); ^{13}C NMR (400 MHz, DMSO-d_6) *δ*: 14.21 (2C), 117.18 (2C), 126.31, 127.14, 127.70, 140.12, 141.43, 142.55, 145.05, 146.32, 146.78, 147.56 (2C), 171.72.

*4.3.2.5. Synthesis and characterization of final compounds: Substituted 5,5′-(quinoxaline-2,3-diyl)bis(thiazol-2-amine) (**8g-n**)*

*4.3.2.5.1. 5,5′-(quinoxaline-2,3-diyl)bis(N,4-diphenylthiazol-2-amine) (**8g**)*. To a solution of 2,3-bis(bromomethyl)quinoxaline (1.0 eq) **2a** in THF, addition of *N,N*-diethyl-*N*'-(phenylcarbamothioyl)benzimidamide **4a** (2.0 eq) was done. Drop wise addition of trimethylamine (1.1 eq) was carried out. Reaction was allowed to proceed at room temperature for 3 h. After completion of reaction, reaction mixture was poured into ice cold water to get the precipitates of compound **8g**. **8g** was purified by column chromatography (Ethyl acetate: Hexane = 1:4). Yellow solid; Yield: 89%; Purity: 99.4%; Melting point: > 250 °C; Molecular

formula: $C_{38}H_{26}N_6S_2$; LC-ESI-MS (*m/z*): 631.1 $[M + H]^+$; IR (KBr, cm^{-1}): 3250.5, 3067.3, 1539.26, 1137.09; ^1H NMR (400 MHz, DMSO-d_6) *δ*: 6.979–7.054 (m, 6H), 7.152–7.227 (m, 6H), 7.351 (t, *J* = 7.6 Hz, 4H), 7.548 (d, *J* = 8.0 Hz, 4H), 7.816–7.840 (m, 2H), 7.981–8.001 (m, 2H), 10.255 (s, D_2O exchangeable, 2H); ^{13}C NMR (400 MHz, DMSO-d_6) *δ*: 117.23 (2C), 118.54 (2C), 121.45 (2C), 127.17 (2C), 127.84 (2C), 127.97 (2C), 128.10 (2C), 128.25 (2C), 128.81 (2C), 129.01 (2C), 130.06 (2C), 135.13 (2C), 139.91 (2C), 139.99 (2C), 140.81 (2C), 147.11 (2C), 148.73 (2C), 162.08 (2C), 164.12 (2C).

*4.3.2.5.2. 5,5′-(quinoxaline-2,3-diyl)bis(thiazol-2-amine) (**8h**).* Final compound **8h** was synthesized as per the procedure described in **8g** using starting materials 2,3-bis(bromomethyl)quinoxaline **2a** and *N*′-carbamothioyl-*N*,*N*-dimethylformimidamide **6a**. **8h** was purified by column chromatography (Chloroform: Methanol = 9.5:0.5). Yellow solid; Yield: 81%; Purity: 98.7%; Melting point: 160–162 °C; Molecular formula: $C_{14}H_{10}N_6S_2$; LC-ESI-MS (*m/z*): 327.2 $[M + H]^+$; IR (KBr, cm^{-1}): 3452.42, 3356.9, 3014.8, 1469.76, 700.12; ^1H NMR (400 MHz, DMSO-d_6) *δ*: 7.510 (s, 2H), 7.588 (s, D_2O exchangeable, 4H), 7.684 (t, *J* = 6.8, 2H), 7.848 (d, *J* = 6.8 Hz, 2H); ^{13}C NMR (400 MHz, DMSO-d_6) *δ*: 123.26 (2C), 127.73 (2C), 129.45 (2C), 139.17 (2C), 141.87 (2C), 144.86 (2C), 171.18 (2C).

*4.3.2.5.3. 5,5′-(quinoxaline-2,3-diyl)bis(N-phenylthiazol-2-amine) (**8i**).* Final compound **8i** was synthesized as per the procedure described in **8g** using starting materials 2,3-bis(bromomethyl) quinoxaline **2a** and *N*,*N*-dimethyl-*N*′-(phenylcarbamothioyl) formimidamide **6b**. **8i** was purified by column chromatography (Ethyl acetate: Hexane = 2:3). Yellow solid; Yield: 68%; Purity: 99.7%; Melting point: 155–157 °C; Molecular formula: $C_{26}H_{18}N_6S_2$; LC-ESI-MS (*m/z*): 479.1 $[M + H]^+$; HRMS (TOF) *m/z* calcd for $C_{26}H_{18}N_6S_2$ $[M + H]^+$ 479.1034, found: 479.1081; IR (KBr, cm^{-1}): 3291.51, 3018.9, 1442.66, 756.23; ^1H NMR (400 MHz, DMSO-d_6) *δ*: 6.9940 (t, *J* = 7.36 Hz, 2H), 7.2127 (t, *J* = 7.4 Hz, 4H), 7.6726–7.7387 (m, 6H), 7.7560 (s, 2H), 7.9375 (d, *J* = 6.4 Hz, 2H), 10.5465 (s, D_2O exchangeable, 2H); ^{13}C NMR (400 MHz, DMSO-d_6) *δ*: 117.54 (4C), 121.80 (2C), 124.55 (2C), 127.92 (2C), 128.69 (2C), 128.79 (2C), 129.65 (2C), 139.52 (2C), 140.48 (2C), 141.21 (2C), 144.48 (2C), 165.89 (2C).

*4.3.2.5.4. 5,5′-(quinoxaline-2,3-diyl)bis(N-(4-fluorophenyl)thiazol-2-amine) (**8j**).* Final compound **8j** was synthesized as per the procedure described in **8 g** using starting materials 2,3-bis(bromomethyl) quinoxaline **2a** and *N*′-((4-fluorophenyl)carbamothioyl)-*N*,*N*-dimethylformimidamide **6c**. **8j** was purified by column chromatography (Ethyl acetate: Hexane = 3:7). Yellow solid; Yield: 72%; Purity: 99.8%; Melting point: > 250 °C; Molecular formula: $C_{26}H_{16}F_2N_6S_2$; LC-ESI-MS (*m/z*): 515.1 $[M + H]^+$; IR (KBr, cm^{-1}): 3207.76, 3045.69, 1507.43, 828.48; ^1H NMR (400 MHz, DMSO-d_6) *δ*: 7.752 (s, 2H), 7.761–7.777 (m, 4H), 7.786–7.872 (m, 4H), 7.917 (t, *J* = 8 Hz, 2H), 8.042 (d, *J* = 6.4 Hz, 2H), 10.684 (s, D_2O exchangeable, 2H); ^{13}C NMR (400 MHz, DMSO-d_6) *δ*: 115.09, 115.16, 115.31, 119.09, 119.17, 119.39, 119.46, 124.64, 125.69, 127.88, 129.46, 129.63, 130.68, 136.90, 136.92 (2C), 137.35, 139.47, 140.42, 140.97, 143.45, 144.39, 144.44, 156.04, 158.43, 165.88, 166.56.

*4.3.2.5.5. 5,5′-(quinoxaline-2,3-diyl)bis(N-(4-chlorophenyl)thiazol-2-amine) (**8k**).* Final compound **8k** was synthesized as per the procedure described in **8g** using starting materials 2,3-bis(bromomethyl) quinoxaline **2a** and *N*′-((4-chlorophenyl)carbamothioyl)-*N*,*N*-dimethylformimidamide **6d**. **8k** was purified by column chromatography (Ethyl acetate: Hexane = 3:7). Yellow solid; Yield: 81%; Purity: 99.9%; Melting point: > 250 °C; Molecular formula: $C_{26}H_{16}Cl_2N_6S_2$; LC-ESI-MS (*m/z*): 546.1 $[M]^+$, 548.1 $[M + 2]^+$, 550.1 $[M + 4]^+$; HRMS (TOF) *m/z* calcd for $C_{26}H_{16}Cl_2N_6S_2$ $[M]^+$ 546.0255, found: 546.0235 $[M]^+$, 548.0188 $[M + 2]^+$, 550.0231 $[M + 4]^+$; IR (KBr, cm^{-1}): 3375.57, 2914.57, 1532.51, 763.84; ^1H NMR (400 MHz, DMSO-d_6) *δ*: 7.326 (s, 2H), 7.342 (d, *J* = 6.9 Hz, 4H), 7.701–7.764 (m, 6H), 7.946 (d, *J* = 6.4 Hz, 2H), 10.705 (s, D_2O exchangeable, 2H); ^{13}C NMR (400 MHz, DMSO-d_6) *δ*: 118.90 (4C), 124.97 (2C), 125.34 (4C), 128.01 (2C), 128.68 (2C), 129.97 (2C), 139.36 (2C), 139.54 (2C), 141.16 (2C), 144.44 (2C), 165.38 (2C).

*4.3.2.5.6. 5,5′-(6-chloroquinoxaline-2,3-diyl)bis(thiazol-2-amine) (**8l**).* Final compound **8l** was synthesized as per the procedure described in **8g** using starting materials 2,3-bis(bromomethyl)-6-chloroquinoxaline **2b** and *N*′-carbamothioyl-*N*,*N*-dimethylformimidamide **6a**. **8l** was purified by column chromatography (Ethyl acetate: Hexane = 1:1). Yellow solid; Yield: 86%; Purity: 99.0%; Melting point: 158–160 °C; Molecular formula: $C_{14}H_9ClN_6S_2$; LC-ESI-MS (*m/z*): 360.1 $[M]^+$, 362.1 $[M + 2]^+$; HRMS (TOF) *m/z* calcd for $C_{14}H_9ClN_6S_2$ $[M]^+$ 360.0019, found: 360.0045 $[M]^+$, 362.0024 $[M + 2]^+$; IR (KBr, cm^{-1}): 3310.95, 3224.16, 1622.20, 1486.22, 826.53; ^1H NMR (400 MHz, DMSO-d_6) *δ*: 7.6103 (s, 2H), 7.796 (s, D_2O exchangeable, 4H), 7.822 (d, *J* = 2.4 Hz, 1H), 7.8634 (s, 1H), 7.882 (d, *J* = 2.4 Hz, 1H); ^{13}C NMR (400 MHz, DMSO-d_6) *δ*: 123.18, 123.29, 126.07, 128.68, 129.31, 133.34, 136.80, 142.09, 144.96, 148.04, 150.59, 171.41, 171.63.

*4.3.2.5.7. 5,5′-(quinoxaline-2,3-diyl)bis(N-(p-tolyl)thiazol-2-amine) (**8m**).* Final compound **8m** was synthesized as per the procedure described in **8g** using starting materials 2,3-bis(bromomethyl) quinoxaline **2a** and *N*,*N*-dimethyl-*N*′-(p-tolylcarbamothioyl) formimidamide **6e**. **8m** was purified by column chromatography (Ethyl acetate: Hexane = 2:3). Yellow solid; Yield: 72%; Purity: 99.8%; Melting point: > 250 °C; Molecular formula: $C_{28}H_{22}N_6S_2$; LC-ESI-MS (*m/z*): 507.1 $[M + H]^+$; HRMS (TOF) *m/z* calcd for $C_{28}H_{22}N_6S_2$ $[M + H]^+$ 507.1347, found: 507.1272; IR (KBr, cm^{-1}): 3388.11, 2923.25, 1533.47, 1217.14, 815.92; ^1H NMR (400 MHz, DMSO-d_6) *δ*: 2.277 (s, 6H), 7.148 (d, *J* = 8.4 Hz, 4H), 7.349 (s, 2H), 7.551 (d, *J* = 8.4 Hz, 4H), 7.748 (t, *J* = 6.4 Hz, 2H), 7.940 (d, *J* = 7.32 Hz, 2H), 10.53 (s, 2H); ^{13}C NMR (400 MHz, DMSO-d_6) *δ*: 20.36 (2C), 117.75 (4C), 124.18 (2C), 127.96 (2C), 129.43 (2C), 129.98 (4C), 131.03 (2C), 138.07 (2C), 139.42 (2C), 141.47 (2C), 144.62 (2C), 166.06 (2C).

*4.3.2.5.8. 5,5′-(6,7-dimethylquinoxaline-2,3-diyl)bis(thiazol-2-amine) (**8n**).* Final compound **8n** was synthesized as per the procedure described in **8g** using starting materials 2,3-bis(bromomethyl)-6,7-dimethylquinoxaline **2c** and *N*′-carbamothioyl-*N*,*N*-dimethylformimidamide **6a**. **8n** was purified by column chromatography (Ethyl acetate: Hexane = 1:1). Yellow solid; Yield: 71%; Purity: 99.6%; Melting point: 110–112 °C; Molecular formula: $C_{16}H_{14}N_6S_2$; LC-ESI-MS (*m/z*): 355.1 $[M + H]^+$; HRMS (TOF) *m/z* calcd for $C_{16}H_{14}N_6S_2$ $[M + H]^+$ 355.0721, found: 355.0789; IR (KBr, cm^{-1}): 3298.42, 3150.23, 1493.93, 12119.06, 871.88; ^1H NMR (400 MHz, DMSO-d_6) *δ*: 2.436 (s, 6H), 7.442 (s, 2H), 7.639 (s, D_2O exchangeable, 4H), 7.675 (s, 2H); ^{13}C NMR (400 MHz, DMSO-d_6) *δ*: 19.71 (2C), 123.47 (2C), 127.08 (2C), 141.14 (2C), 143.87 (2C), 144.81 (2C), 148.05 (2C), 171.25 (2C).

4.4. Biological activity

4.4.1. In vitro BACE-1 enzyme inhibition assay

BACE-1 inhibitory trends of test compounds **8a-8n** were checked through *in vitro* enzyme inhibition assays. For this purpose, Corning 96 Well Black Polystyrene well-plates were used and a total volume of 100 μL, per well was added to facilitate enzyme-substrate reaction. The other enzymatic reaction contents included 4.0 ng/μL of human recombinant BACE-1 enzyme (procured form BioVision Inc., India), 50 μM substrate (MCA-SEVNLDAEFR-Ednp-KRR-NH_2·3TFA), various concentrations of the test compound (100 μM, 10 μM and 1 μM, dissolved in DMSO) and 0.1 M sodium-acetate buffer (pH 4.5). After addition of all these reagents, fluorescence readings were recorded by Varioskan Flash multimode plate reader under excitation and emission wavelength of 320 nm and 405 nm, respectively and were termed as zero hour reading. The plate was then incubated for 2 h at 37 °C and fluorescence was recorded again. % inhibition of BACE-1 enzyme was determined through calculations and IC_{50} values [denoted as μM ± SEM (n = 3)] of all test compounds were obtained. These data are denoted as mean of 3 determinations ± SEM and compared with

standard compound's (AZD3839) reported Ki value of 26.1 nmol/L [40], as enumerated in Table 3.

4.4.2. Animals and treatments

Animal care and all *in vivo* experiments were conducted after sanctioned from Institutional Animal Ethics Committee (Approval No: PERD/IAEC/2016/049 & PERD/IAEC/2016/050). The experiments were carried out in harmony with internationally approved good laboratory practices (GLP) for housing and for the handling of animals CPCSEA guidelines (Committee for the Purpose of Control and Supervision of Experiments on Animals, Govt. of India) were strictly followed. Sprague-Dawley rats (female, 4–6 months old, 150–200 g body weight) were housed in well ventilated cages at standard conditions of relative humidity (60 ± 5%), temperature (25 ± 3 °C), 12:12 h light/dark cycle and 10% air exhaust conditioning unit were maintained. Animals were housed in group of 3 rats per cage in animal house (at B. V. Patel PERD Centre, Ahmedabad) with unrestricted access to food and water. All behavioural experiments were conducted in a semi-soundproof and semi-dark laboratory between 10 am and 6 pm being the active phase of rodents. Animals were deprived of food overnight prior to the surgical procedures and sacrificed.

4.4.3. In vivo analysis

4.4.3.1. Acute anti-inflammatory activity: Carrageenan induced rat paw edema study. Carrageenan induced rat paw edema model is widely used model for determination of anti-inflammatory activity [50]. A series of 14 test compounds were screened to determine their acute inflammatory potentials using a carrageenan induced rat paw edema model. 17 groups (n = 6) denoted as normal control (NC), disease control (DC), positive control (PC) and 14 test groups (**8a-8n**) were randomly grouped and used for the study. For pre-dosing, all test compounds (50 mg kg^{-1}) and PC (7.5 mg $kg^{-1}$of diclofenac, Sigma Aldrich) were administered orally as 0.2% agar suspension. The NC and DC groups were fed with vehicle (0.2% agar suspension) only. Edema was induced by subcutaneously injecting 0.1 mL of 1% carrageenan (Spectrochem; solution in normal saline) into left hind paw of rats, after 1 h of oral dosing. The alteration in their paw volume before and after 3 h of carrageenan injection was measured using a mercury plethesmometer [50]. The % edema inhibition of paw was calculated by using the following equation:

$$\% \text{ edema inhibition} = [\{(V_t/V_0)_{DC} - (V_t/V_0)_{treated}\}/(V_t/V_0)_{DC}] \times 100$$

where

V_t = rat paw volume at 3rd h
V_0 = rat paw volume at 0th h

% edema inhibition data are represented as mean ± SEM (n = 6 animals/group) and statistical analysis was performed utilizing GraphPad Prism software (GraphPad Software, San Diego, CA, USA) by one-way analysis of variance (ANOVA) was used to detect significant effect of treatment, followed by Tukey's multiple comparison test ($^*p < 0.05$).

4.4.3.2. Chronic anti-inflammatory activity: Formalin induced rat paw edema study. Out of 14 compounds, 4 compounds (**8c**, **8g**, **8l** and **8n**) were taken forward to check their potential activity on chronic inflammation model [50]. Animals were divided into random groups of seven (n = 6) designated as NC, DC, PC and 4 test groups (**8c**, **8g**, **8l** and **8n**). In this model, rats were orally pre-dosed with celecoxib (≥98%, Sigma Aldrich, 40 mg·kg^{-1}) for PC group and with test compounds (50 mg·kg^{-1}) as 0.2% agar (HiMedia) suspension. NC and DC groups received vehicle only (0.2% agar suspension). Posterior to 1 h of oral dosing, animals were subcutaneously injected 0.1 mL of 2% formalin (SD Fine Chemicals; in normal saline) in the sub plantar region of their left hind paw. Oral dosing and subcutaneous injections were continued for 5 consecutive days. Paw volume measurements were recorded before and after 5 h of formalin administration using mercury plethesmometer [50]. % inhibition of edema in rat paw was calculated using following equation:

$$\% \text{ edema inhibition} = [\{(V_t/V_0)_{DC} - (V_t/V_0)_{treated}\}/(V_t/V_0)_{DC}] \times 100$$

where

V_t = rat paw volume at 5th h
V_0 = rat paw volume at 0th h

The data are represented as mean % edema inhibition ± SEM (n = 6 animals/group) and statistical analysis was performed by one-way ANOVA followed by Tukey's multiple comparison test ($^*p < 0.05$).

4.4.3.3. Aluminium chloride induced Alzheimer's disease model. The highest active test compound **8n** apparent from BACE-1 inhibition assay, acute and chronic inflammation models was further assessed for its anti-Alzheimer's activity. Compound **8n** was screened through behavioural parameters, antioxidant property and histopathological studies to shed light onto its anti-Alzheimer's propensity. Animals were divided into 4 groups (n = 6) designated as NC, DC, PC and test groups (**8n**). The PC group was pre-dosed orally with meloxicam (as meloxicam sodium salt hydrate, Sigma Aldrich, 5 mg·kg^{-1}) whereas the test group with test compound **8n** (50 mg·kg^{-1}) prepared in 0.2% agar suspension for 28 days. NC and DC groups received vehicle only. After oral dosing of compounds, animals were injected with aluminium chloride (Sigma Aldrich; 4.2 mg·kg^{-1} i.p.*)* for 28 days. This model has been in use for several years [41]. The described procedures were repeated for 28 days and during this period following studies were carried out.

4.4.3.3.1. Estimation of behavioural parameters. Behavioural parameters were scrutinized using Y-maze test, pole climbing apparatus and elevated plus maze test. Animals were trained for 5 days ahead of the *intra-peritonial* $AlCl_3$ administration. Thereafter behavioural parameters were recorded during training and retention sessions on the 7th, 14th, 21st and 28th day of $AlCl_3$ induced rat model.

Y-maze test. Y-maze test works on the principle of immediate working memory of rodents. It assesses the rodent's tendency to explore novel environment as they preferably choose to visit the unexplored region over previously visited region and this peculiar behavior is scientifically measured in terms of 'simultaneous alteration performance' (SAP). SAP was observed using Y maze apparatus [37]. Y-maze was made up of 3 identical wooden arms (40 × 9 × 16 cm) and placed on an evenly planar area at an angle of 120° with respect to each other. In our experiment, each arm was labeled as 'A', 'B', and 'C', respectively. Experimental rats were placed at the end of one arm and allowed to explore the maze environment for 5 min. Arm entries were recorded visually like A, B and C. SAP was calculated as total number of entries minus two, and the % alteration is calculated as (actual correct alteration ÷ maximum alteration) × 100. Data are given as mean % alteration ± SEM and statistical analysis was performed by two-way ANOVA test followed by multiple comparisons of Tukey's test. Statistical significance was measured as $^*p < 0.05$ compared to NC and as $^{\#}p < 0.05$ compared to DC.

Conditioned avoidance response test. In rats, the conditioned avoidance response (CAR) was assessed by using Cook's pole climbing apparatus made up of a sound proof wooden chamber having dimensions 25 × 25 × 25 cm [51]. Electric shock was delivered by a metallic bar located on the chamber's floor. A shock-proof pole of diameter 2.5 cm was equipped at the core of chamber. Study was initiated by placing a rat inside the apparatus and 45 s time was stipulated to each rat in-order to explore the chamber's internal environment. After that, conditioned stimulus was delivered using buzzer signal for 10 s and unconditioned stimulus was delivered by giving electric shock for 45 s.

The rats were trained for 3 consecutive days with 1st day 5 trials, 2nd day 3 trials and 3rd day 1 trial. During training session rats learned to escape the floor shock by climbing up the pole after the buzzer signal and the time duration taken by them is termed as conditioned avoidance response (CAR). CAR was recorded for each rat during retention session, which had 1 trial of experiment on 7th, 14th, 21st and 28th day in $AlCl_3$ model. Data were represented as (mean ± SEM) and statistical analysis was performed by two-way ANOVA test followed by multiple comparisons of Tukey's test. Statistical significance was measured as $^{*}p < 0.05$ compared to NC and $^{\#}p < 0.05$ compared to DC.

Elevated plus maze test. Elevated plus maze (EPM) test works on the principle of aversion of rodents towards heights and open space environment. Animals naturally tend to escape from open spacious region and high altitudes and prefer to adobe in closed or rather safe environment [38]. In our experiment, EPM test was availed to check the spatial working memory of rats and time taken to find the closed arm location was measured. The EPM assembly was framed up by wooden arms; two open arms (29 × 5 cm) and two enclosed arms (29 × 5 × 15 cm) were connected by a central platform (5 × 5 cm) elevated at a height of 40 cm with respect to the floor. During the training session which lasted for 5 days each rat was kept at one open arm facing away from central platform and allowed to explore the maze environment for 5 min. Open arm entries, enclosed arm entries, total entries, % time spent in open arm and % time spent in enclosed arm were noted down. Transfer latencies were recorded during retention session on 7th, 14th, 21st and 28th day of the $AlCl_3$ model. Data were calculated by two-way ANOVA test followed by multiple comparisons of Tukey's test (mean ± SEM). Statistical significance was measured as $^{*}p < 0.05$ when compared to NC and ($^{\#}p < 0.05$) compared to DC.

4.4.3.3.2. Haematological parameters estimation. Haematological parameters were measured after 28 days of treatment. On 29th day, rats were anaesthetized by isoflurane. Blood samples were collected in 1 mL heparinized micro centrifuge tubes from the retro orbital sinus of rats. Automated haematology analyser (VetScan HM-5; Abaxis Inc., Union City, CA, USA) was used for estimation of haemoglobin and haematocrit level [39].

4.4.3.3.3. Estimation of serum biochemical parameters. Blood samples were collected from retro orbital sinus in 1 mL non-heparinized micro centrifuge tubes. Serum was separated from the blood samples and biochemical parameters like % albumin and total protein was estimated by an automated analyser (Transasia EM 360) [39].

4.4.3.3.4. Antioxidant activity. After 28 days of treatment, on the 29th day animals were euthanized, their intact brains were removed by cervical dislocation and washed with saline to remove traces of blood. The brain samples were divided into two hemispheres and used for lipid peroxidase and superoxide dismutase assays.

Lipid peroxidase (LPO) assay. Brain tissues from all rats were taken into Hank's balanced salt solution (HBSS) of pH 7.4 and homogenized at 5000 rpm for 3 cycles (30 s each) using Polytron homogenizer (Kinematica, Switzerland). The homogenized samples were centrifuged at 35,000 rpm for 10 min using Sorvall, legend X1R centrifuge. From each centrifuged sample, its supernatant was discarded and pellet was re-suspended in 0.1 mL of HBSS which was further used for LPO assay. The LPO activity was measured by reaction of malonaldehyde (MDA): thiobarbituric acid (TBA). The assay reaction contained 0.1 mL of tissue homogenate (as processed earlier), 2 mL of 8.1% sodium dodecyl sulfate, 1.5 mL of 20% acetic acid (pH was adjusted to 3.5 using 1 M NaOH), and 1.5 mL of 0.8% aqueous TBA solution. Further, 0.7 mL of double distilled water was added to the reaction mixture and volume was adjusted up to 4 mL. The reaction mixtures were heated up to 95 °C for 1h in water bath. 5 mL of *n*-butanol: pyridine (15:1 v/v) mixture and 1 mL of double distilled water was added to it. The contents were first vortexed and then centrifuged at 3000 rpm for 7 min. The supernatant obtained after centrifugation was collected and processed further for MDA detection. Formation of MDA in the supernatant was measured at a wavelength of 532 nm in UV/visible spectrophotometer (Shimadzu UV-1800). Extinction coefficient of MDA (1.45×10^{-5}/min/cm) was used for calculation [39,41].

LPO was calculated using following formula:

$$\text{LPO} = [(\text{Sample} - \text{Blank}) \times 145] \times 10^{-5}/\text{weight of organ (gram)}$$

Superoxide dismutase (SOD) assay. The brain tissues were further processed for SOD activity assay. Tissues were taken in 2 mL of chilled Tris buffer (50 mM, pH 8.2 was adjusted using 2 mM EDTA) homogenized for 3 cycles (30 *sec*). The homogenates were treated with 0.1% of Triton × 100 (1 mL) at 4 °C for 30 min. Each sample was again subjected to homogenization at 5600 rpm for 30 min at 4 °C. The supernatant obtained was separated and used for SOD activity. Further, the supernatant was divided into two parts one stored at 4–8 °C and the other heated in water bath at 95 °C for 1 h. Absorbance readings were recorded after 0th and 9th min of pyrogallol (HiMedia) addition to each sample [41,42]. The calculations were done using per gram fresh tissue weight. SOD enzyme activity was evaluated by the following equation:

$$\text{Enzyme activity (units mg}^{-1}\text{of fresh tissue weight)} = [(\Delta B - \Delta E)/\Delta P] \times 120$$

where

ΔB = boiled sample absorbance per min (9th min. reading – 0th min. reading)
ΔE = cold sample absorbance per min (9th min. reading – 0th min. reading)
ΔP = pyrogallol control per min (9th min. reading – 0th min. reading)

4.4.3.4. Histopathological studies of rat brain. For histopathological studies, brain samples were collected and stored in formalin (in 10% neutral buffer) solution for 24 h. Brain sections were stained using Congo-red and Haematoxylin-Eosin (HE) stains and transferred to transparent glass slides. These were observed under optical microscope (ProgRes C3 OLYMPUS, U-TV1X, Japan) and images were captured using Progres capture Pro 2.9.0.1 software.

4.4.3.5. Gastrointestinal (GI) safety study. Gastrointestinal safety study was carried out only for **8n** due to its maximal activity amongst all hybrid molecules. On the 29th day of treatment, euthanized animals were subjected to GI dissection. Stomach and intestines were removed from the digestive system and washed with chilled 0.01 M phosphate buffer saline (pH 7.4) and stored in sterile tubes. These viscera were preserved for 24 h in 10% neutral buffered formalin. In the next step, samples were washed with 70% ethanol (v/v). Each sample was checked for hemorrhagic damages using digital vernier caliper (Absolute AOS Digimatic; Mitutoyo, Japan). Further, gastric damage was calculated in terms of lesion index. Also, histopathological observations were done using HE stained sections of stomach and intestines [43,44].

Acknowledgements

All authors thank B. V. Patel PERD Centre for providing research facilities. S.R.S. thanks DST-INSPIRE for providing fellowship to carry out research work. S.R.S. and N.B.P. thank NIRMA University for registering as research scholar. Authors thank Professor V. K. Jain, Department of Chemistry, University School of Sciences, Gujarat University for extending the facility of Schrödinger software.

Funding Sources

Authors thank B. V. Patel Pharmaceutical Education and Research Development (PERD) Centre for financial support. SRS thanks DST-INSPIRE, Govt. of India for providing fellowship to carry out research work.

Declaration of Competing Interest

The authors state no conflict of interest.

Appendix A. Supplementary material

Results of docking studies and copies of ^{1}H NMR and ^{13}C NMR spectra of compounds **8a-8n** are provided in Supplementary Material. ^{1}H NMR spectra of intermediates **2a** and **4a** are also provided.

Supplementary data to this article can be found online at https://doi.org/10.1016/j.bioorg.2019.102992.

References

[1] L.C. Lu, J.H. Bludau, Alzheimer's Disease, Greenwood Press, Santa Barbara, CA, 2011.
[2] D.E. Barnes, K. Yaffe, The projected effect of risk factor reduction on Alzheimer's disease prevalence, Lancet Neurol. 10 (2011) 819–828.
[3] M. Prince, A. Wimo, M. Guerchet, G.C. Ali, Y.T. Wu, M. Prina, World Alzheimer Report 2015—The Global Impact of Dementia: An analysis of prevalence, incidence, cost and trends, 2015, Alzheimer's Disease International (ADI), London, 2017.
[4] Alzheimer's Association, 2017 Alzheimer's Disease Facts and Figures, Alzheimer's & Dementia 13 (2017) pp. 325–373.
[5] D.J. Selkoe, D. Schenk, Alzheimer's disease: molecular understanding predicts amyloid-based therapeutics, Annu. Rev. pharmacol. Toxicol. 43 (2003) 545–584.
[6] A. Dagher, C. Bleicher, J.a. Aston, R.N. Gunn, P.B. Clarke, P. Cumming, Reduced dopamine D1 receptor binding in the ventral striatum of cigarette smokers, Synapse 42 (2001) 48–53.
[7] X. Li, H. Wang, Z. Lu, X. Zheng, W. Ni, J. Zhu, Y. Fu, F. Lian, N. Zhang, J. Li, H. Zhang, Development of multifunctional pyrimidinylthiourea derivatives as potential anti-Alzheimer agents, J. Med. Chem. 59 (2016) 8326–8344.
[8] M.I. Choudhary (Ed.), Drug Design and Discovery in Alzheimer's Disease, Elsevier, 2015.
[9] S. Lee, X. Zheng, J. Krishnamoorthy, M.G. Savelieff, H.M. Park, J.R. Brender, J.H. Kim, J.S. Derrick, A. Kochi, H.J. Lee, C. Kim, Rational design of a structural framework with potential use to develop chemical reagents that target and modulate multiple facets of Alzheimer's disease, J. Am. Chem. Soc. 136 (2013) 299–310.
[10] J.S. Derrick, R.A. Kerr, Y. Nam, S.B. Oh, H.J. Lee, K.G. Earnest, N. Suh, K.L. Peck, M. Ozbil, K.J. Korshavn, A. Ramamoorthy, A redox-active, compact molecule for cross-linking amyloidogenic peptides into nontoxic, off-pathway aggregates: in vitro and in vivo efficacy and molecular mechanisms, J. Am. Chem. Soc. 137 (2015) 14785–14797.
[11] F.I. Baptista, A.G. Henriques, A.M. Silva, J. Wiltfang, O.A. da Cruz e Silva, Flavonoids as therapeutic compounds targeting key proteins involved in Alzheimer's disease, ACS Chem. Neurosci. 5 (2014) 83–92.
[12] S.Y. Li, X.B. Wang, S.S. Xie, N. Jiang, K.D. Wang, H.Q. Yao, H.B. Sun, L.Y. Kong, Multifunctional tacrine–flavonoid hybrids with cholinergic, β-amyloid-reducing, and metal chelating properties for the treatment of Alzheimer's disease, Eur. J. Med. Chem. 69 (2013) 632–646.
[13] E. Viayna, I. Sola, M. Bartolini, A. De Simone, C. Tapia-Rojas, F.G. Serrano, R. Sabaté, J. Juárez-Jiménez, B. Pérez, F.J. Luque, V. Andrisano, Synthesis and multitarget biological profiling of a novel family of rhein derivatives as disease-modifying anti-Alzheimer agents, J. Med. Chem. 57 (2014) 2549–2567.
[14] E. Nepovimova, E. Uliassi, J. Korabecny, L.E. Pena-Altamira, S. Samez, A. Pesaresi, G.E. Garcia, M. Bartolini, V. Andrisano, C. Bergamini, R. Fato, Multitarget drug design strategy: quinone–tacrine hybrids designed to block amyloid-β aggregation and to exert anticholinesterase and antioxidant effects, J. Med. Chem. 57 (2014) 8576–8589.
[15] C. Rochais, C. Lecoutey, F. Gaven, P. Giannoni, K. Hamidouche, D. Hedou, E. Dubost, D. Genest, S. Yahiaoui, T. Freret, V. Bouet, Novel multitarget-directed ligands (MTDLs) with acetylcholinesterase (AChE) inhibitory and serotonergic subtype 4 receptor (5-HT4R) agonist activities as potential agents against Alzheimer's disease: the design of donecopride, J. Med. Chem. 58 (2015) 3172–3187.
[16] R. Morphy, C. Kay, Z. Rankovic, From magic bullets to designed multiple ligands, Drug Discov Today 9 (2004) 641–651.
[17] A. Cavalli, M.L. Bolognesi, A. Minarini, M. Rosini, V. Tumiatti, M. Recanatini, C. Melchiorre, Multi-target-directed ligands to combat neurodegenerative diseases, J. Med. Chem. 51 (2008) 347–372.
[18] Z. Wang, Y. Wang, B. Wang, W. Li, L. Huang, X. Li, Design, synthesis, and evaluation of orally available clioquinol-moracin M hybrids as multitarget-directed ligands for cognitive improvement in a rat model of neurodegeneration in Alzheimer's disease, J. Med. Chem. 58 (2015) 8616–8637.
[19] S.R. Sagar, D.P. Singh, N.B. Panchal, R.D. Das, D.H. Pandya, V. Sudarsanam, M. Nivsarkar, K.K. Vasu, Thiazolyl-thiadiazines as Beta Site Amyloid Precursor Protein Cleaving Enzyme-1 (BACE-1) Inhibitors and Anti-inflammatory Agents: Multitarget-Directed Ligands for the Efficient Management of Alzheimer's Disease, ACS Chem. Neurosci. 9 (2018) 1663–1679.
[20] J. Cummings, T. Morstorf, G. Lee, Alzheimer's drug-development pipeline: 2016, Alzheimer's Dement. Transl. Res. Clin. Interv. 2 (2016) 222–232.
[21] A. Agis-Torres, M. Sölhuber, M. Fernandez, J.M. Sanchez-Montero, Multi-target-directed ligands and other therapeutic strategies in the search of a real solution for Alzheimer's disease, Curr. Neuropharmacol. 12 (2014) 2–36.
[22] M. Bajda, N. Guzior, M. Ignasik, B. Malawska, Multi-target-directed ligands in Alzheimer's disease treatment, Curr. Med. Chem. (2011) 4949–4975.
[23] F. Sorrentino Prati, G. Bottegoni, M.L. Bolognesi, A. Cavalli, BACE-1 inhibitors : from recent single-target molecules to multitarget compounds for Alzheimer 's disease, J. Med. Chem. (2017), https://doi.org/10.1021/acs.jmedchem.7b00393.
[24] K. Chiang, E.H. Koo, Emerging therapeutics for Alzheimer's disease, Annu. Rev. Pharmacol. Toxicol. 54 (2014) 381–405.
[25] J.M. Rubio-Perez, J.M. Morillas-Ruiz, A review: inflammatory process in Alzheimer's disease, role of cytokines, Sci. World J. (2012).
[26] C.K. Glass, K. Saijo, B. Winner, M.C. Marchetto, F.H. Gage, Mechanisms underlying inflammation in neurodegeneration, Cell 140 (2010) 918–934.
[27] A. Crowe, C. Ballatore, E. Hyde, J.Q. Trojanowski, V.M.Y. Lee, High throughput screening for small molecule inhibitors of heparin-induced tau fibril formation, Biochem. Biophys. Res. Commun. 358 (2007) 1–6.
[28] N.S. Honson, R.L. Johnson, W. Huang, J. Inglese, C.P. Austin, J. Kuret, Differentiating Alzheimer disease-associated aggregates with small molecules, Neurobiol. Dis. 28 (2007) 251–260.
[29] W. Huang, L. Tang, Y. Shi, S. Huang, L. Xu, R. Sheng, P. Wu, J. Li, N. Zhou, Y. Hu, Searching for the multi-target-directed ligands against Alzheimer's disease: Discovery of quinoxaline-based hybrid compounds with AChE, H 3 R and BACE 1 inhibitory activities, Bioorg. Med. Chem. 19 (2011) 7158–7167.
[30] P.X. Franklin, A.D. Pillai, P.D. Rathod, S. Yerande, M. Nivsarkar, H. Padh, K.K. Vasu, V. Sudarsanam, 2-Amino-5-thiazolyl motif: A novel scaffold for designing anti-inflammatory agents of diverse structures, Eur. J. Med. Chem. 43 (2008) 129–134.
[31] A.D. Pillai, P.D. Rathod, F.P. Xavier, H. Padh, V. Sudarsanam, K.K. Vasu, Tetra substituted thiophenes as anti-inflammatory agents: Exploitation of analogue-based drug design, Bioorg. Med. Chem. 13 (2005) 6685–6692.
[32] R.S. Giri, H.M. Thaker, T. Giordano, B. Chen, S. Nuthalapaty, K.K. Vasu, V. Sudarshanam, Synthesis and evaluation of quinazolinone derivatives as inhibitors of NF-κB, AP-1 mediated transcription and eIF-4E mediated translational activation: Inhibitors of multi-pathways involve in cancer, Eur. J. Med. Chem. 45 (2010) 3558–3563.
[33] Glide, Maestro 11.1.012, Schrödinger, LLC, New York, NY, 2017.
[34] Qikprop, Maestro 11.1.012, Schrödinger, LLC, New York, NY, 2017.
[35] R.P. Hullin, J. Miller, W.F. Short, Amidines. part V. preparation of amidines from cyanides and substituted aminomagnesium halides, J. Chem. Soc. 12 (1947) 394.
[36] H.B. Jalani, A.N. Pandya, D.H. Pandya, J.A. Sharma, V. Sudarsanam, K.K. Vasu, An efficient one-pot synthesis of functionally diverse 2-aminothiazoles from isothiocyanates, amidines/guanidines and halomethylenes, Tet. Lett. 54 (2013) 5403–5406.
[37] Z. Suo, A.A. Cox, N. Bartelli, I. Rasul, B.W. Festoff, R.T. Premont, G.W. Arendash, GRK5 deficiency leads to early Alzheimer-like pathology and working memory impairment, Neurobiol. Aging 28 (2007) 1873–1888.
[38] L. Liu, I.J. Orozco, E. Planel, Y. Wen, A. Bretteville, P. Krishnamurthy, L. Wang, M. Herman, H. Figueroa, W.H. Yu, O. Arancio, K. Duff, A transgenic rat that develops Alzheimer's disease-like amyloid pathology, deficits in synaptic plasticity and cognitive impairment, Neurobiol. Dis. 31 (2008) 46–57.
[39] D.P. Singh, S.P. Borse, M. Nivsarkar, A novel model for NSAID induced gastroenteropathy in rats, J. Pharmacol. Toxicol. Methods 78 (2016) 66–75.
[40] F. Jeppsson, S. Eketjäll, J. Janson, S. Karlström, S. Gustavsson, L.L. Olsson, A.C. Radesäter, B. Ploeger, G. Cebers, K. Kolmodin, B.M. Swahn, S. Von Berg, T. Bueters, J. Fälting, Discovery of AZD3839, a potent and selective BACE1 inhibitor clinical candidate for the treatment of alzheimer disease, J. Biol. Chem. 287 (2012) 41245–41257.
[41] K.D. Parekh, R.P. Dash, A.N. Pandya, K.K. Vasu, M. Nivsarkar, Implication of novel bis-imidazopyridines for management of Alzheimer's disease and establishment of its role on protein phosphatase 2A activity in brain, J. Pharm. Pharmacol. 65 (2013) 1785–1795.
[42] S. Marklund, G. Marklund, Involvement of the superoxide anion radical in the autooxidation of pyrogallol and a convenient assay for superoxide dismutase, Eur. J. Biochem. 47 (1974) 469–474.
[43] D.P. Singh, S.P. Borse, M. Nvsarkar, Co-administration of quercetin with pantoprazole sodium prevents NSAID-induced severe gastroenteropathic damage efficiently: Evidence from a preclinical study in rats, Exp. Toxicol. Pathol. 69 (2017) 17–26.
[44] D.P. Singh, S.P. Borse, M. Nivsarkar, Overcoming the exacerbating effects of ranitidine on NSAID-induced small intestinal toxicity with quercetin: Providing a complete GI solution, Chem. Biol. Interact. 272 (2017) 53–64.
[45] U. Eidhoff, F. Zink, U. Hassiepen, N. Ostermann, O. Simic, U. Hommel, S. Worpenberg, B. Gerhartz, Crystal structure of human BACE2 in complex with a hydroxyethylamine transition-state inhibitor, J. Mol. Biol. 355 (2006) 249–261.
[46] A.Y. Lee, S.V. Gulnik, J.W. Erickson, Conformational switching in an aspartic proteinase, Nat. Struct. Mol. Biol. 5 (1998) 866–871.
[47] SiteMap, Maestro 11.1.012, Schrödinger, LLC, New York, NY, 2017.
[48] G. Rimon, R.S. Sidhu, D.A. Lauver, J.Y. Lee, N.P. Sharma, C. Yuan, R.A. Frieler,

R.C. Trievel, B.R. Lucchesi, W.L. Smith, Coxibs interfere with the action of aspirin by binding tightly to one monomer of cyclooxygenase-1, Proc. Natl. Acad. Sci. 107 (2010) 28–33.

[49] J.L. Wang, D. Limburg, M.J. Graneto, J. Springer, J.R.B. Hamper, S. Liao, J.L. Pawlitz, R.G. Kurumbail, T. Maziasz, J.J. Talley, J.R. Kiefer, J. Carter, The novel benzopyran class of selective cyclooxygenase-2 inhibitors. Part 2: The second clinical candidate having a shorter and favorable human half-life, Bioorganic Med. Chem. Lett. 20 (2010) 7159–7163.

[50] A.D. Pillai, P.D. Rathod, P.X. Franklin, M. Patel, M. Nivsarkar, K.K. Vasu, H. Padh, V. Sudarsanam, Novel drug designing approach for dual inhibitors as anti-inflammatory agents: Implication of pyridine template, Biochem. Biophys. Res. Commun. 301 (2003) 183–186.

[51] M.L.G. Wadenberg, P.B. Hicks, The conditioned avoidance response test re-evaluated: Is it a sensitive test for the detection of potentially atypical antipsychotics? Neurosci. Biobehav. Rev. 23 (1999) 851–862.